ELSEVIER

Contents lists available at ScienceDirect

# **Computers and Chemical Engineering**

journal homepage: www.elsevier.com/locate/cace





# Enabling the direct solution of challenging computer-aided molecular and process design problems: Chemical absorption of carbon dioxide

Ye Seol Lee, Amparo Galindo, George Jackson, Claire S. Adjiman \*

Department of Chemical Engineering, Sargent Centre for Process Systems Engineering, Institute for Molecular Science and Engineering, Imperial College London, South Kensington Campus, London, SW7 2AZ, United Kingdom

### ARTICLE INFO

#### Keywords:

Computer-aided molecular and process design Mixed-integer nonlinear programming Amine solvent design  $\mathrm{CO}_2$  chemical absorption process SAFT- $\nu$  Mie

### ABSTRACT

The search for improved  $CO_2$  capture solvents can be accelerated by deploying computer-aided molecular and process design (CAMPD) techniques to explore large molecular and process domains systematically. However, the direct solution of the integrated molecular-process design problem is very challenging as nonlinear interactions between physical properties and process performance render a large proportion of the search space infeasible. We develop a methodology that enables the direct and reliable solution of CAMPD for absorption–desorption processes, using the state-of-the-art SAFT- $\gamma$  Mie group contribution approach to predict phase and chemical equilibria. We develop new feasibility tests and show them to be highly efficient at reducing the search space, integrating them in an outer-approximation algorithm. The framework is applied to design an aqueous solvent and  $CO_2$  chemical absorption–desorption process, with 150 CAMPD instances across three case studies solved successfully. The optimal solvents are more promising than those obtained with sequential molecular design approaches.

### 1. Introduction

Carbon dioxide (CO2) is one of the primary anthropogenic greenhouse gases that directly contributes to a negative impact on the environment and life on our planet. A significant reduction in total CO<sub>2</sub> emissions is essential to limit the rise in the global average temperature to 2 °C, as has been highlighted in several Intergovernmental Panel on Climate Change (IPCC) reports (IPCC, 2021). In December 2015, the 21st conference of the parties (COP21) agreement set out the highly ambitious aspiration of limiting the temperature increase to 1.5 °C by 2050 (UNFCCC, 2015). In response to this, there have been growing efforts to develop and adopt low-carbon options to reduce net CO2 emissions to the atmosphere. Carbon Capture and Storage (CCS) technologies are widely regarded as playing a vital role in a portfolio of net-zero emissions, and are expected to contribute approximately 20% of the reductions in greenhouse gas emissions by 2035 (IEA, 2011). Among the variety of available CCS technologies, post-combustion capture based on the chemical absorption of CO2 in an amine solvent is regarded as one of the most promising technologies in terms of technological maturity, applicability and capability of handling exhaust streams from large point industrial sources (Chao et al., 2021). An amine-based solvent that has been widely used for the process is an aqueous monoethnaolamine (MEA) solution due to its high reaction rate with CO2, moderate absorption capacity and low solvent cost.

However, the main disadvantages of using this conventional solvent include: high energy requirements associated with solvent regeneration, which takes up to 50% of the total energy use of the process; harmful environmental and health impacts; and high operational costs resulting from limited  $\rm CO_2$  solubility (Borhani and Wang, 2019; Wang and Song, 2020)

To counter these shortcomings, considerable efforts have been expended on the search for alternative amine-based solvents that have better thermal, economic and environmental performance. The identification, characterization and assessment of candidate solvents are challenging due to the large number of potential solvent molecules and the significant influence of the choice of solvent on process performance, meaning that optimal solvents can only be identified by considering the interactions between the molecular and process-level decisions simultaneously. Indeed, the importance of considering multiple effects rather than focusing on standard metrics such as equilibrium absorption capacity has been well recognized (Mota-Martinez et al., 2017).

In this context, Computer-Aided Molecular and Process Design (CAMPD) offers a systematic framework to evaluate a very wide range of molecular structures in terms of system metrics, given a set of desirable physicochemical properties and process performance criteria (Adjiman et al., 2014). A variety of solution strategies have been developed

E-mail address: c.adjiman@imperial.ac.uk (C.S. Adjiman).

Corresponding author.

Nomenclature	
Nomenciature	
Sets	
A1	Set of violated constraints
$G_A,G_{\mathrm{CH}_2}$	Set of amine functional groups and functional groups that include $\mathrm{CH}_2$
$G_{ m iso}$	Set of function groups that include CH or C
IC NC	Set of components in the system, i.e. N.C.
	Set of components in the system, i.e., $NC = \{N_2, CO_2, H_2O, solvent\}$
NC'	Set of components considered in Test 2, i.e., $NC' = \{\text{solvent}, H_2O\}$
Superscripts	
*	Optimal solution
k	Iteration numbers
U, L	Upper and lower bounds
Symbols	
$\alpha, \beta, \gamma$	Phase fractions of vapor, first liquid, and second liquid at equilibrium
$n_S$	Vector that represents the number of occurrences of the SAFT- $\gamma$ Mie groups
n	Vector of functional groups defining the molecular structure
$y, x_{\beta}, x_{\gamma}$	Mole fractions in the vapor, first liquid and second liquid phases at equilibrium
z	Total composition of the system
$\Delta T_{\min}$	Minimum approach temperature in heat exchangers (K)
μ	Viscosity of the mixture of solvent and water (cP)
$ heta_0$	Lean loading (mol mol <sup>-1</sup> )
$LC_{50,\mathrm{mgL}}$	Lethal dose concentration of the solvent (mg ${\rm L}^{-1}$ )
$MW_i$	Molecular weight of component $i \in NC$ (g mol <sup>-1</sup> )
$P_{N_a}, P_{N_d}$	Operating pressures at the last stage of absorber and desorber (MPa)
$Q_{ m total}$	Total energy consumption per ton of CO <sub>2</sub> captured (GJ ton-CO <sub>2</sub> <sup>-1</sup> )
$Q_{\mathrm{reb}}, Q_{\mathrm{cond}}$	Energy consumption in the reboiler and condenser of the desorber (MW)
$T_0$	Lean solvent temperature (K)
$T_{ m dew}$	Dew point temperature of the mixture of solvent and water (K)
$T_{ m AIT}$	Auto-ignition temperature of the solvent (K)
$T_{ m bp}$	Normal boiling temperature of the solvent (K)
$T_{ m cond}$	Condenser temperature (K)
$T_{ m fp}$	Flash point temperature of the solvent (K)

for CAMPD problems, focusing on handling the numerical complexity arising from the inherent non-convexity of structure–property and process models and the combinatorial nature of the problem arising from the use of molecular structure as an optimization variable. The reader is referred to Ng et al. (2015), Austin et al. (2016), Papadopoulos et al. (2018) and references therein for an in-depth description of a variety of solution strategies and their performance. Unfortunately,

Normal melting temperature of the solvent (K)
Operating temperature at the last stage of absorber and desorber (K)
Operating temperature of the chemical absorption–desorption process (K)
Solvent handling temperature (K)
Solvent mass fraction of the binary mixture of the solvent and water (g $g^{-1}$ )
Total annualized cost, total cost of investment, and total operating cost ( $\$$ million year $^{-1}$ )

many algorithms encounter computational difficulties with the large-scale mixed-integer nonlinear problem (MINLP) formulations that are typical of CAMPD problems. This is mainly because: (1) the relationship between process performance and molecular structure exhibits highly nonlinear behavior making it prohibitively expensive and challenging to find a solution of the multiscale model; (2) the design space formed by the integrated solvent-process model is characterized by the presence of infeasible subregions, so that it is not possible for standard optimization algorithms to identify a feasible solution for many solvent structures without a high-quality starting point. To enable the widespread application of CAMPD to CO<sub>2</sub> capture processes, there is a pressing need to develop robust CAMPD algorithms that allow one to avoid infeasibilities during the exploration of a large design space (Adjiman et al., 2021).

One class of methods suited to overcoming the aforementioned infeasibilities is that of decomposition-based approaches. In these methods, the process and molecular design are decoupled and treated as a series of separate subproblems. Each subproblem is often formulated with a different level of complexity and a reduced size of the design space in order to make the problem tractable. Note that the term "decomposition" in this context refers to the overall strategy for solving the CAMPD problem rather than the solution approach for the solution of the MINLP.

Hostrup et al. (1999) proposed a hybrid method for the integrated design of solvents and environmentally-benign separation processes. They first used thermodynamic insights and knowledge of the system to eliminate less attractive solvents and process flowsheet options. The remaining candidate solvents and flowsheet structures were then optimized based on a selected objective function. A similar CAMPD solution approach was adopted by Roughton et al. (2012) for the identification of new liquid entrainers for extractive distillation processes to improve energy efficiency. Karunanithi et al. (2006) developed a decompositionbased CAMPD framework for the design of optimal solvents and solvent mixtures for the crystallization of ibuprofen, consisting of the solution of several subproblems: the first subproblem was formulated as a computer-aided molecular design (CAMD) problem aiming to reduce the discrete solvent search space by evaluating molecular structural constraints, pure component properties, and mixture properties and miscibility. Subsequently, an MINLP CAMPD problem was solved for the reduced search domain. Papadopoulos and Linke (2006b,a) developed a CAMPD framework that decouples the original MINLP problem into two subproblems: a multi-objective optimization (MOO) method was employed to screen Pareto-optimal solvents with respect to key molecular properties, and a molecular clustering approach that integrates the process and molecular design was then applied to select solvents from the set of identified Pareto-optimal solvents. This method has been extended by Papadopoulos et al. (2010, 2013) for the design of optimal working fluids and working fluid mixtures for organic Rankine cycle (ORC) processes and by Kokossis and Yang (2010) for the synthesis and design of future biorefineries.

A reverse approach to decomposition was outlined by Eden et al. (2004) and Eljack et al. (2007). In these studies, molecular properties were optimized to maximize process performance, such as an economic value of the process, without considering discrete decisions (i.e., molecular structure). Subsequently, molecular structures that match the identified property targets as closely as possible were explored by solving a property-matching CAMD problem (Maranas, 1997). Bommareddy et al. (2010) incorporated a similar strategy using a group contribution method (Marrero and Gani, 2001) for the representation of molecular property operators. Within the family of property-targeting approaches, Bardow et al. (2010) and Oyarzún et al. (2011) proposed a continuous molecular targeting-computer-aided molecular design (CoMT-CAMD) to integrate molecular design and process design, using the perturbed-chain statistical associating fluid theory (PC-SAFT) (Gross and Sadowski, 2001) as the property model. In the first stage, a model of the process was used to optimize the continuous parameters characterizing the molecules within the PC-SAFT equation of state and process variables. The optimal parameters describe a hypothetical molecule which was then mapped onto an existing molecule in the second stage. The performance of the proposed method was demonstrated for the design of solvents for pre-combustion CO<sub>2</sub> capture (Stayrou et al., 2014; Lampe et al., 2015), and the design of organic Rankine cycle fluids (Lampe et al., 2014, 2015).

While there have been encouraging advances in decomposition-based CAMPD techniques that allow for the generation of optimal molecular candidates, some drawbacks of these methods have also been discussed by Ng et al. (2015), Gopinath et al. (2016), Austin et al. (2016), and Schilling et al. (2020). A major disadvantage of decomposition-based methods is that they can result in suboptimal solutions if the heuristic or expert judgment made in the initial step (introduced to reduce the search space) does not capture all process options. Therefore, the quality of the solutions is often highly dependent on the formulation of the subproblems. Unfortunately, it is not always straightforward to decompose the original problem into several subproblems. To overcome this, direct solution approaches that aim to solve the full CAMPD problem have been receiving increasing attention.

Burger et al. (2015) proposed a hierarchical approach to address the numerical difficulties in the solution of direct CAMPD problems. Good initial guesses for the integrated solvent and process design of physical absorption process for CO<sub>2</sub> removal from a methane stream were generated using an MOO technique applied to a simplified CAMPD problem. The Pareto-optimal solvent candidates obtained were then used as starting points for the solution of the full CAMPD MINLP, with the detailed process model. One difficulty in applying this method is that there is no guarantee that the Pareto-optimal solvents represent points that are near-optimal or even feasible in the full CAMPD model. Furthermore, the solution of the simplified design problem may itself be very challenging due to the presence of highly nonideal phase behavior and nonlinear structure—property model equations.

An enumeration strategy has been proposed by Scheffczyk et al. (2018), who introduced the COSMO-CAMPD framework, a generate-and-test approach in which process performance is evaluated for all molecular candidates that satisfy certain constraints. Candidates were generated via a genetic algorithm and their properties evaluated by COSMO-RS (Klamt et al., 2010). Candidate molecules were screened using thermodynamic feasibility tests and an assessment via pinch-based models. Candidates were then re-evaluated with a more detailed COSMO-RS model and assessed through more rigorous process models. The framework has since been expanded to embed cradle-to-grave environmental assessment of solvents within the COSMO-susCAMPD framework (Fleitmann et al., 2021).

With a view to making the problem more tractable, Pereira et al. (2011) solved a simplified version of the CAMPD problem for the design of solvent and process for the physical absorption of  $CO_2$  from a methane stream. The problem was posed as a continuous optimization problem in which solvent mixtures of n-alkanes were represented in

terms of their average chain length making use of the congruence properties of the n-alkanes. The need for binary variables for the representation of molecules was avoided by choosing an equation of state parameter, the chain length, as an optimization variable. This, however, came at the cost of a restricted solvent design space. Zhou et al. (2017) adopted a direct solution approach for a CAMPD MINLP via a hybrid stochastic-deterministic optimization approach. In their methodology, a genetic algorithm (GA) was applied to generate molecular candidates and a gradient-based nonlinear programming (NLP) algorithm was used to optimize the process for a given set of molecular candidates. The effectiveness of the method was tested on the design of a solvent and process for CO2 physical absorption. Although robustness of the algorithm was demonstrated, there were several difficulties when applying it to more complex systems. Firstly, this approach did not address the issue that, in the optimization of the process model for a fixed solvent, one needs to make sure that the molecules are feasible with respect to the specified process configurations. When generating a new set (population) of molecules with the GA, the selection of feasible or high-performance molecules becomes very difficult if many of generated molecules violate the process constraints. Moreover, increases in the population size greatly increase the computational cost.

Schilling et al. (2017a) introduced a 1-stage CoMT-CAMD approach, building on their earlier work on two-stage CoMT-CAMD (Bardow et al., 2010). The MINLP problem was solved using an outer approximation (OA) algorithm (Duran and Grossmann, 1986) to identify optimal hypothetical working fluids, with the use of PC-SAFT, and associated ORC process conditions. The same approach was applied to the design of working fluid *mixtures* for the ORC process (Schilling et al., 2020). While the applicability of the method seems promising, the formulation of the problem was developed based on the reverse approach which requires the molecular mapping of the hypothetical molecular structure to a real molecule in a final step. The actual performance of the molecules found by reverse mapping deviated from that of the hypothetical working fluids (Schilling et al., 2017b).

An alternative strategy for the simultaneous approach is outlined by Gopinath et al. (2016). Motivated by the work of Buxton et al. (1999), the authors developed a set of feasibility tests and incorporated them into an OA algorithm. The feasibility tests serve as a pre-processing step before solution of the primal problem, through which infeasible molecules and process operating conditions can be eliminated from the search space without tackling the more challenging process optimization problem. By automatically detecting infeasibilities as a function of molecular structure, they found that not only was convergence to an optimal solution achieved regardless of user-provided initial guesses, but that computational efficiency was also improved without making significant model simplifications or introducing any approximations or reductions of the process and molecular design space. The robustness of the algorithm was validated by application to the design of solvent and process for the physical absorption of CO<sub>2</sub> from high-pressure natural gas. The concept of physical reduction of the domain was also implemented in integrated working fluid and ORC process design (Bowskill et al., 2020), with appropriate feasibility tests, and resulted in similarly improved robustness and efficiency as demonstrated by the exploration of a space of 58,000 possible fluids. Finally, initial work on deploying this approach for the chemisorption of CO<sub>2</sub> was reported by Lee et al. (2021).

In our current paper, we build on the work of Gopinath et al. (2016), Bowskill et al. (2020) and Lee et al. (2021) and propose a robust optimization framework for the simultaneous design of optimal aqueous amine solvent and process combinations for  $\mathrm{CO}_2$  capture from flue gas, without limiting the level of detail in the representation of molecular structures, thermodynamic models, and process models. This represents a significant challenge as chemisorption via amine solvents is considerably more complex than physical absorption in terms of the underpinning physicochemical phenomena and process units, with the presence of chemical reactions and solvent regeneration taking place

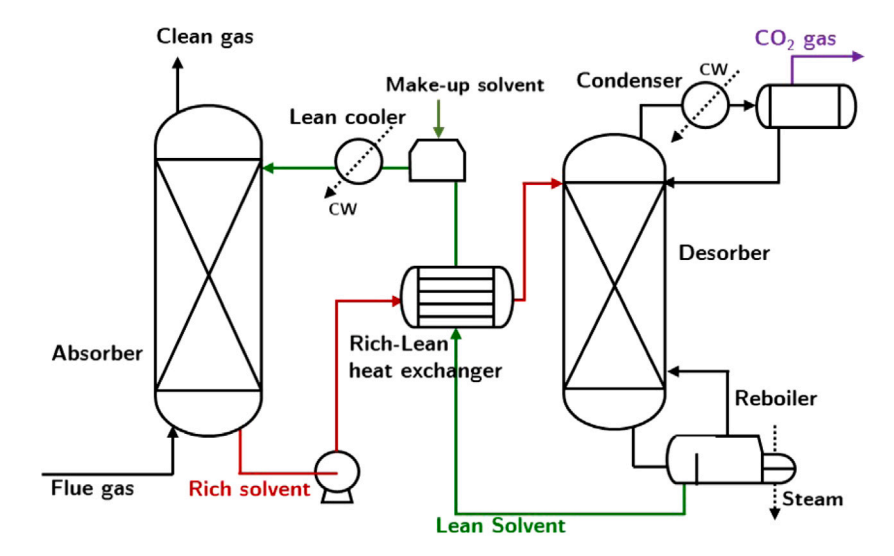


Fig. 1. Overview of the CO2 absorption-desorption process configuration.

via a desorber rather than a flash unit. We introduce tailored feasibility tests that are applicable to any chemisorption process and incorporate them into the OA algorithm (Duran and Grossmann, 1986) for the solution of CAMPD problems such that large molecular and process design spaces are explored simultaneously without difficulty. The design of the feasibility tests is focused on recognizing the feasible domain based on: (1) the physicochemical properties of the pure candidate solvent and aqueous solvent mixture; (2) an assessment of the suitability of a candidate solvent based on an analysis of the phase behavior of mixtures of the solvent(s); and CO<sub>2</sub> (3) an assessment of the suitability of the solvent mixture to meet the target degree of separation. The performance of the proposed algorithm is highlighted through several CAMPD instances focused on the chemical absorption-desorption of CO<sub>2</sub>. The CAMPD optimization formulation is developed based on the process model introduced in Lee (2022), and Lee et al. (2023) and the SAFT-y Mie group contribution equation of state (EOS) (Papaioannou et al., 2014; Dufal et al., 2014) is applied to facilitate the reliable prediction of the physical properties and phase behavior of the water-solvent-CO2 mixtures, using recently developed models for the mixtures of interest (Khalit, 2019; Haslam et al., 2020; Perdomo et al., 2021, 2023). For each case study, an economic criterion is used to evaluate the performance of the solvent/process combinations and to identify optimal designs.

# 2. Problem formulation

### 2.1. Overall problem statement

For the formulation of the integrated design problem that encompasses solvent and chemical absorption process optimization, we make use of the process and cost models that were developed and validated in Lee (2022), Lee et al. (2023). Given a solvent design space,  $\rm CO_2$  absorption–desorption process specifications, constraints and a suitable objective function, an MINLP CAMPD optimization problem is formulated to determine an optimal combination of aqueous amine solvent and process conditions. The generic mathematical formulation of the MINLP problem is as follows:

$$\min_{x,n} \quad f(x,n) 
s.t. \quad g(x,n) \le 0 
\quad h(x,n) = 0 
\quad Cn \le d 
\quad x \in \mathbb{R}^m, \ n \in N \subset \mathbb{Z}^q$$
(1)

where x is an m-dimensional vector of continuous variables, n is a q-dimensional vector of integer variables that define the molecular space, g(x,n) is a vector of inequality constraints that represent design constraints and feasibility constraints, h(x,n) is a vector of equality constraints that include structure–property models and process models, and the set of linear equations  $Cn \le d$  represents molecular constraints such as the octet rule (Odele and Macchietto, 1993) and bounds on vector n.

### 2.2. CO<sub>2</sub> chemical absorption process model

The process configuration is shown in Fig. 1. A flue gas leaving a direct contact cooler (not shown in the Figure) is fed into the bottom of an absorber. The gas stream flows upward through the packed bed inside the absorber, against a countercurrent stream of aqueous amine solvent. The gaseous CO2 is chemically absorbed into the amine solution and the clean gas stream leaving the top of the absorber is emitted to the atmosphere. The CO2-rich solution leaving the bottom of the absorber passes thorough a rich-lean heat exchanger (HE) where the CO<sub>2</sub>-rich amine solution is heated by the hot CO<sub>2</sub>-lean amine solution. It then enters the top of a desorber for solvent regeneration. The CO<sub>2</sub>rich amine solution flows downward against a counter-current flow of water-rich vapor generated in the reboiler, until CO2 concentration in the solvent solution is reduced to the target level. Finally, the CO<sub>2</sub>lean amine solution passes through the rich-lean HE and lean cooler to achieve a pre-defined operating temperature and then returns to the top of the absorber.

The flue gas is assumed to arise from a 400 MWe combined-cycle gas-turbine (CCGT) power plant (Bailey and Feron, 2005). The model inputs and process specification used in the current study are listed in Table 1.

The equilibrium-stage model proposed in Lee (2022), Lee et al. (2023) is used to represent the process. For brevity, the model and modeling assumptions are not reprised here but some salient points are highlighted. Specifically, the absorber and desorber are modeled as a series of equilibrium stages via mass, equilibrium, summation and heat (MESH) equations. The complex phase and chemical equilibria on each stage are modeled using an implicit approach within the SAFT- $\gamma$  Mie framework, wherein the formation of reaction products such as carbamate and bicarbonate is treated as the association of the reactant species (amine solvent and  $CO_2$ ). This approach has been demonstrated to represent the phase and chemical behavior of these systems well (Mac Dowell et al., 2010) for the molecular SAFT-VR SW equation of state (Gil-Villegas et al., 1997), which is suitable

Table 1
Input values and baseline process specifications of a CO<sub>2</sub> capture process model for a 400MWe CCGT power plant (Bailey and Feron, 2005). The loading is defined as moles of CO<sub>2</sub> absorbed in 1 mole of amine solvent.

Base line process specification	Units	Value
Lean solvent flow rate	$m^3 h^{-1}$	23
MEA concentration in lean solvent	wt %	30.4
Absorber inlet flue gas flow rate	$Nm^3 h^{-1}$	1,800,000
Absorber inlet flue gas CO2 molar composition	mol%	5
Absorber inlet flue gas H2O molar composition	mol%	12
Absorber inlet flue gas N2 molar composition	mol%	83
Absorber inlet flue gas temperature	K	323.15
Absorber operating pressure	MPa	0.101
Temperature approach in heat exchangers	K	10
Lean solvent temperature, $T_0$	K	313.15
Desorber operating pressure, $P_{N_d}$	MPa	0.181
Lean loading, $\theta_0$	$mol mol^{-1}$	0.25
Condenser temperature, $T_{\rm cond}$	K	333.15
Degree of CO <sub>2</sub> captured	%	90

for solvents for which experimental data are available, and to yield reliable predictions of the mole fractions of ionic species at different conditions (Rodriguez et al., 2012) and of the process behavior (Alhajaj et al., 2016). Through extension to group contribution versions of SAFT (Chremos et al., 2016; Perdomo et al., 2021, 2023), the predictive capabilities of the approach have been expanded to large classes of solvents. An advantage of the implicit approach is that only the species that are fed to the process (nitrogen, water, CO<sub>2</sub>, amine solvent) need to be modeled explicitly, thereby reducing the number of material balances and variables needed. Finally, nearly all thermodynamic properties, including stream enthalpies and heat of absorption, are modeled using SAFT-γ Mie, so that a consistent thermodynamic framework is used and no assumptions of ideality are required. To enable equipment sizing, the stream viscosity and surface tension are predicted using the method proposed by Hsu et al. (2002) and Hukkerikar et al. (2012b).

In order to improve the convergence behavior of the process model, a tailored initialization strategy proposed by Lee (2022), Lee et al. (2023) and based on the concept of the inside-out algorithm (Boston, 1980; Russell, 1983) introduced in conjunction with the process model. This approach has been found to lead to reliable convergence for a range of (feasible) candidate solvents in extensive parametric and optimization studies. Finally, the model has been extensively validated against pilot plant data and found to provide good agreement with key process metrics, including CO<sub>2</sub> removal and energy requirements (Lee, 2022; Lee et al., 2023).

As for the process optimization problem, the objective function is set as the total annualized cost (TAC), which is a metric of overall economic performance, and three continuous variables are considered as degrees of freedom: the temperature of the solvent entering the absorber ( $T_0$ ), the lean-solvent loading ( $\theta_0$ ) defined as the moles of CO<sub>2</sub> absorbed in one mole of amine solvent in the CO<sub>2</sub>-lean stream entering the absorber, and the desorber pressure ( $P_{N_d}$ ). The set of design variables also includes the solvent structure as defined by n.

# 2.3. Solvent design space

The molecular design space is defined by groups that are present in typical  $\mathrm{CO}_2$  capture solvents, and for which group-contribution interaction parameters are available for the group-contribution methods used. The following 13 functional groups are included:  $\mathrm{NH}_2\mathrm{CH}_2$ ,  $\mathrm{NH}_2\mathrm{CH}$ ,  $\mathrm{NH}_2\mathrm{C}$ ,  $\mathrm{NH}\mathrm{CH}_3$ ,  $\mathrm{NH}\mathrm{CH}_2$ ,  $\mathrm{NH}\mathrm{CH}$ ,  $\mathrm{NCH}_3$ ,  $\mathrm{NCH}_2$ ,  $\mathrm{CH}_3$ ,  $\mathrm{CH}_2$ ,  $\mathrm{CH}_3$ ,  $\mathrm{CH}_2$ ,  $\mathrm{CH}_3$ ,  $\mathrm{CH}_3$ ,  $\mathrm{CH}_2$ ,  $\mathrm{CH}_3$ ,

used, a set of linear equations is formulated to translate the functional groups defining the molecular structure, described by the vector n, into a vector  $n_S$  through which the number of occurrences of the following SAFT-γ Mie groups is specified: NH<sub>2</sub>, NH, N, CH<sub>3</sub>, CH<sub>2</sub>, CH, C, CH<sub>2</sub>OH,  $\mathrm{NH_2^*}$ ,  $\mathrm{NH^*}$ ,  $\mathrm{N^*}$ ,  $\mathrm{CH_2OH_{Short}}$ . The larger group  $\mathrm{CH_2OH}$  is introduced to provide improved accuracy relative to adopting smaller groups such as CH<sub>2</sub> and OH (Hutacharoen et al., 2017; Chremos et al., 2016; Khalit, 2019; Haslam et al., 2020; Perdomo et al., 2021) by accounting for the polarization of the CH2 when close to a hydroxyl group. The groups NH<sub>2</sub>\*, NH\*, N\*, CH<sub>2</sub>OH<sub>Short</sub> represent second-order groups, which can be used more effectively to capture proximity effects and the polarizing effect of water. In the context of SAFT-γ Mie, second-order group effects for the amine groups and hydroxyl groups are considered to account for the different unlike (or cross) interactions, when one of the groups exists in a certain molecular environment (Haslam et al., 2020). Considering MEA, for example, the molecule is defined as  $n_{\text{NH}_2\text{CH}_2} = 1$ ,  $n_{\rm CH_2} = 1$ ,  $n_{\rm OH} = 1$ . This can be translated into an equivalent solvent structure for use in the SAFT- $\gamma$  Mie EOS, i.e.,  $n_{S,NH_2}=1$ ,  $n_{S,CH_2}=1$ ,  $n_{S,CH_2OH_{Short}} = 1.$ 

The use of the two sets of functional groups, n and  $n_S$ , requires the introduction of additional constraints to ensure the equivalence of the structures. For example, the choice of SAFT groups means that OH can only appear in the molecule within the CH<sub>2</sub>OH group (or the CH<sub>2</sub>OH<sub>Short</sub> group), as captured by the following additional constraint:

$$\sum_{j \in G_{\text{CH}_1}} n_j \ge n_{\text{OH}},\tag{2}$$

where  $G_{\text{CH}_2}$  is the set of functional groups that include CH<sub>2</sub> given by  $G_{\text{CH}_2} = \{\text{NCH}_2, \text{NHCH}_2, \text{NH}_2\text{CH}_2, \text{CH}_2\}$ .

Such constraints ensure that the mapping between the two representations of a given molecule is consistent. The molecular design space is thus defined as the intersection of the sets of molecules that can be represented using vectors n and  $n_S$  and the rules and constraints that define allowable combinations of groups. Because of the differences in the sizes of the groups in the two representations, the mapping is not one-to-one. Consider, for example, methyldiethanolamine (MDEA), which can be defined with two different n vectors,  $n_{\text{MDEA},1} = (n_{\text{NCH}_3} =$  $1, n_{\text{CH}_2} = 4, n_{\text{OH}} = 2)$  and  $n_{\text{MDEA},2} = (n_{\text{NCH}_2} = 1, n_{\text{CH}_2} = 3, n_{\text{CH}_3} = 1)$  $1, n_{OH} = 2$ ), and a unique  $\mathbf{n}_S$  vector in the SAFT- $\gamma$  Mie environment, i.e.,  $\mathbf{n}_{S,\text{MDEA}}=(n_{S,\text{N}}=1,n_{S,\text{CH}_2}=3,n_{S,\text{CH}_3}=1,n_{S,\text{CH}_2\text{OH}_{S,\text{hort}}}=1).$  In some group-contribution methods (e.g., Marrero and Gani (2001)), there are clear rules for choosing amongst duplicates, for instance by favoring larger groups. In other cases, such as the methods used in our work, the two representations are valid and will give different predictions for the properties of interest and hence different overall performance. If one or both representations are found to yield high performance, then the molecule should be investigated further to resolve the uncertainty inherent in the group-contribution methods. Further details of the mapping between two different sets of groups and the associated constraints can be found in Appendix A.1.

An equality constraint is introduced to ensure molecular feasibility of the acyclic compounds (Odele and Macchietto, 1993):

$$\sum_{i=1}^{N} (2 - v_i) n_i - 2 = 0, \tag{3}$$

where  $v_i$  is the valence of group i.

The total number of functional groups in the molecule is limited by an upper bound,  $n_{\iota}^{U}$ :

$$\sum_{i=1}^{N} n_i - n_t^U \le 0.$$
(4)

The total number of groups with amine functionality is constrained by lower and upper bounds  $[n_{G_A}^L, n_{G_A}^U]$ :

$$n_{G_A}^L \le \sum_{j \in G_A} n_j \le n_{G_A}^U, \tag{5}$$

where  $G_A$  is the set of amine groups given by  $G_A = \{NH_2CH_2, NH_2CH, NH_2C, NHCH_3, NHCH_2, NHCH, NCH_3, NCH_2\}$ . Similarly, the number of hydroxyl groups is constrained by an upper bound  $n_{OH}^U$ :

$$n_{\rm OH} - n_{\rm OH}^U \le 0. \tag{6}$$

With GC-based approaches, the molecular structure is defined by the number of groups of each type appearing in the molecule without taking into account the connectivity, meaning that it is not possible to distinguish some isomers. As a result, isomers represented by the same functional groups are predicted to have identical properties. With this mind, a further constraint that limits the total number of CH and C groups appearing in a solvent to an upper bound  $n_{\rm iso}^U$  is introduced in order to reduce degeneracy as a consequence of having many isomers:

$$\sum_{j \in G_{\rm iso}} n_j - n_{\rm iso}^U \le 0,\tag{7}$$

where  $G_{\rm iso}$  is a set of functional groups that include CH or C given by  $G_{\rm iso}=\{{\rm NHCH,\ NH_2C,\ CH,\ C}\}$ . Finally, the lower and upper bound on each groups are

$$n_i \in \{n_i^L, n_i^U\}, i = 1, \dots, N.$$
 (8)

# 3. Proposed CAMPD algorithm

The main contribution of our current work is a CAMPD framework that enables the simultaneous optimization of solvent and chemical absorption process variables with a detailed equilibrium model and without introducing any reductions of the process or molecular design spaces. A key concept used in the proposed CAMPD approach is the introduction of feasibility tests within an OA framework (Duran and Grossmann, 1986; Fletcher and Leyffer, 1994). In the original OA algorithm, the problem is decomposed into a nonlinear programming (NLP) subproblem, the primal problem, and a mixed-integer linear programming (MILP) subproblem, the master problem. The algorithmic procedure begins by solving the first primal problem for the fixed discrete variables. The master problem is then solved for the approximate design space obtained by linearizing the objective function and active constraints around a set of points identified so far. The solution of the master problem is used to generate new binary variables for the subsequent primal problem. The iterative solution of NLP and MILP continues until the algorithm converges. While the OA was originally designed for problems that are convex in the continuous variables and linear in the binary variables, the introduction of equality relaxation and augmented penalty (OA/ER/AP) (Kocis and Grossmann, 1989; Viswanathan and Grossmann, 1990) has made it applicable to problems that are nonconvex in the continuous variables, albeit without guaranteeing their global solution. The global solution of the type of MINLP considered is in principle possible (e.g., Adjiman et al. (2000)) by solving convex relaxations of the NLPs, but the degree of nonconvexity and scale of the CAMPD problems considered is beyond the scope of current global optimization solvers. Instead, we solve the nonconvex NLPs with a multi-start approach. The OA was chosen because the framework is particularly well suited for implementing the feasibility tests, as the properties of the molecule and the process model are only ever evaluated/optimized for chemically-meaningful molecules. If a branch-and-bound framework were to be used, then expensive computations would have to be carried out for hypothetical molecules (with non-integer group numbers), reducing the usefulness of the proposed feasibility tests. Instead, the OA framework makes it possible to eliminate infeasible process conditions and solvent structures from the search space before solving highly nonlinear (process optimization) primal problems.

The feasibility tests are derived on the basis of physical properties and thermodynamic behavior and are used to determine if the process is feasible for the current solvent/set of discrete variable values without

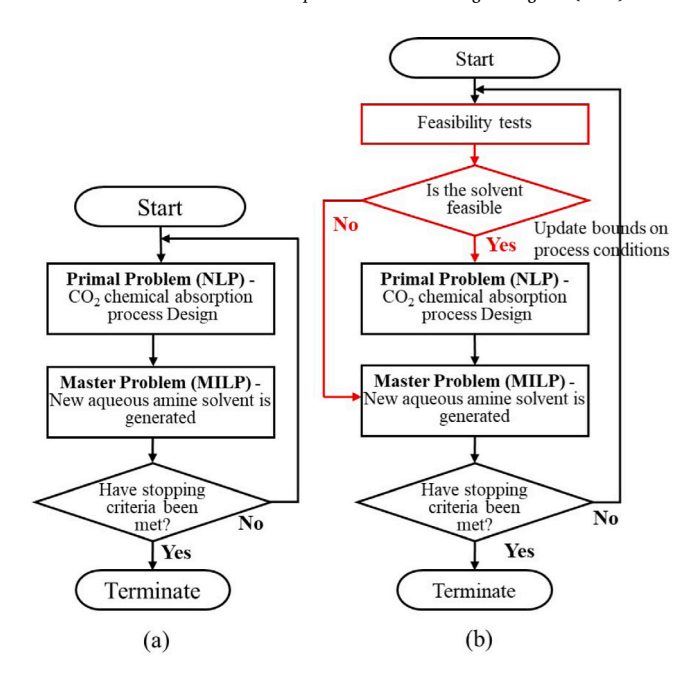


**Fig. 2.** Schematic illustration of (a) a standard outer-approximation algorithm, and (b) the proposed framework with feasibility tests. Red boxes represent the steps introduced in the modified algorithm. This figure is an adaptation of Figure 2 in Bowskill et al. (2020)

solving the full process optimization problem. If the feasibility tests indicate the process is infeasible, the primal problem is bypassed by discarding the solvent from consideration in subsequent iterations, and the master problem is solved to generate a new molecule. If the feasibility tests are passed, the optimal process performance for the fixed solvent is evaluated by solving the primal problem. This approach has recently been shown to be highly effective for the CAMPD of physical absorption processes (Gopinath et al., 2016) and organic Rankine cycles (Bowskill et al., 2020). Flowcharts for the standard OA algorithm and the OA algorithm with the feasibility tests are displayed in Fig. 2. Elements of the proposed algorithm are discussed in more detail in the remainder of this section.

# 3.1. Feasibility tests

In this section, we describe four feasibility tests that can be applied to the CAMPD of chemical absorption processes. The aims of these tests are to determine whether a given solvent is infeasible and to eliminate process conditions that are incompatible with the chemical solvent. In addition, when a solvent is found to pass all the tests, the results are used to set reduced bounds on the process variables and to identify a suitable starting point for the solution of the primal problem.

In order to adapt the feasibility tests proposed by Gopinath et al. (2016) to the more complex setting of the  $\mathrm{CO}_2$  chemical absorption–desorption process, several significant modifications are made, so that the OA algorithm modified with new feasibility tests can reliably generate solutions. Key differences are the formulation of an optimization problem to avoid the formation of two liquid phases in the absorber (Test 2) and several modifications and extensions of the separation feasibility tests of Gopinath et al. (2016) (Tests 3 and 4). These include a reformulation that accounts for the possibility of vapor–liquid–liquid equilibrium (VLLE) and for the presence of chemical reactions; an extension to quaternary systems; and the derivation of new constraints to consider the feasibility of the desorber.

**Table 2** Property prediction methods and bounds on the properties used in Test 1,  $(T_{\rm sh}^L=298.15{\rm K},~T_{\rm sh}^U=308.15~{\rm K},~T_{\rm op}^U=413.15~{\rm K},~\mu^U=0.1\times10^3~{\rm cP}$  (Gopinath et al., 2016) and  $LC_{\rm 50~mol}^U=10$ ).

Physical property	Bounds	Reference
T <sub>bp</sub> (K) at 1 atm	$[T_{\rm sh}^{U},573]$	Papaioannou et al. (2014)
$T_{\text{dew}}$ (K) at 1 atm	$[T_{op}^{T}, 573]$	Papaioannou et al. (2014)
$T_{\rm mp}$ (K) at 1 atm	$[0, T_{\rm sh}^L]$	Hukkerikar et al. (2012b)
$LC_{50,\text{mgL}}$ (mg/L)	$[0, LC_{50,mgL}^{U}]$	Hukkerikar et al. (2012a)
$T_{\rm AIT}$ (K)	$[T_{\rm op}^U, 10^3]$	Hukkerikar et al. (2012b)
$T_{\text{fp}}$ (K)	$[T_{\rm sh}^{1}, 10^{3}]$	Hukkerikar et al. (2012b)
$\mu$ (cP) at $T_{\rm sh}^L$ and 1 atm	$[0, \mu^U]$	Hsu et al. (2002)

### 3.1.1. Test 1: Solvent property feasibility

In Test 1, the properties of the pure candidate solvent n or those of the aqueous solution are evaluated to determine whether they lie within acceptable bounds. In Test 1, seven essential properties (Schilling et al., 2020; Harper et al., 1999) are considered: five pure solvent properties, namely the normal boiling temperature  $(T_{\rm bp})$ , the normal melting point  $(T_{\rm mp})$ , the toxicity as measured by the lethal dose concentration ( $LC_{\rm 50,mgL}$ ), the auto-ignition temperature  $(T_{\rm AIT})$  and the flash point  $(T_{\rm fp})$ , and two mixture properties, namely the dew point temperature  $(T_{\rm dew})$ , and the viscosity  $(\mu)$ . The thermodynamic property models used for the prediction of these properties and their sources are summarized in Table 2.

For solvent handling to be feasible, the normal boiling point  $T_{\rm bp}$  and the normal melting point  $T_{\rm mp}$  of the solvent are constrained by the lower and upper bound on the solvent handling temperature, i.e.,  $T_{\rm sh}^L$  and  $T_{\rm sh}^U$ , respectively. This is to ensure the solvent is in the liquid state when it is transported or stored. The safety of the solvent is evaluated using  $LC_{50,{\rm mgL}}$ ,  $T_{\rm fp}$  and  $T_{\rm AIT}$  and each property is compared with desired ranges, where  $T_{\rm op}^U$  is an upper bound on the operating temperature chosen to avoid solvent degradation. The viscosity of the aqueous amine solvent is limited by  $\mu^U$  in order to make sure that the maximum permissible limit for a centrifugal pump is not exceeded. The viscosity is calculated at the minimum solvent handling temperature  $T_{\rm sh}^L$ . Finally, a lower bound on the process operating temperature  $T_{\rm op}^L$  is imposed on the dew point temperature  $T_{\rm dew}$  to ensure that the lean solvent is in the liquid phase at the absorber inlet. Here, we set  $T_{\rm op}^L$  to be equal to the cooling medium temperature. The resulting formulation of Test 1 is as follows:

$$\begin{split} g_{1,1} &= T_{\rm sh}^U - T_{\rm bp}(P=1 \ {\rm atm}, \textbf{\textit{n}}) \leq 0 \\ g_{1,2} &= T_{\rm mp}(P=1 \ {\rm atm}, \textbf{\textit{n}}) - T_{\rm sh}^L \leq 0 \\ g_{1,3} &= LC_{50,\rm mgL}(\textbf{\textit{n}}) - LC_{50,\rm mgL}^U \leq 0 \\ g_{1,4} &= \mu(T_{\rm sh}^L, P=1 \ {\rm atm}, \textbf{\textit{z}}(\textbf{\textit{n}})) - \mu^U \leq 0 \\ g_{1,5} &= T_{\rm sh}^U - T_{\rm fp}(P=1 \ {\rm atm}, \textbf{\textit{n}}) \leq 0 \\ g_{1,6} &= T_{\rm op}^L - T_{\rm dew}(P=1 \ {\rm atm}, \textbf{\textit{z}}(\textbf{\textit{n}})) \leq 0 \\ g_{1,7} &= T_{\rm op}^U - T_{\rm AIT}(P=1 \ {\rm atm}, \textbf{\textit{n}}) \leq 0 \end{split}$$

where z(n) is the composition of the aqueous solvent mixture, which is fixed at  $W_{0,\text{solvent}}$ , a specific weight fraction of amine solvent. We denote the set of inequality constraints in Test 1 by  $g_1(n) \le 0$ .

It can be seen from the constraints that solvent candidates can be examined via Test 1 regardless of the process design since the properties in Test 1 are independent of the optimal process conditions. The property constraints that are expressed linearly with respect to n, specifically  $g_{1,2}$  and  $g_{1,5}$ , are included in the master problem to increase the likelihood of generating feasible solvent candidates and thus omitted from Test 1 after the first iteration.

# 3.1.2. Test 2: Solvent liquid miscibility

While the work of Gopinath et al. (2016) was focused on pure solvents, the solvents considered here are mixtures that may exhibit undesirable phase behavior such as liquid-liquid equilibria (LLE). Test 2

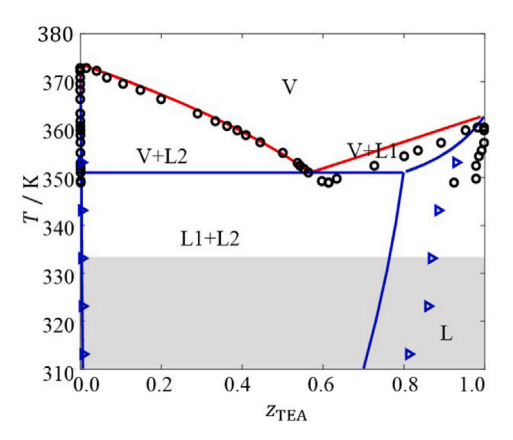


**Fig. 3.** The temperature-mole fraction  $T-z_{\rm TEA}$  fluid phase behavior of a binary mixture of water and TEA at P=0.101 MPa. The liquid-liquid equilibrium region (L1+L2), vapor-liquid equilibrium regions (V+L1 and V+L2) are delimited by the phase boundaries (curves) predicted with the SAFT- $\gamma$  Mie EOS. The black circles (o) correspond to experimental data (Stephenson, 1993) for VLE and the blue triangles (a) to experimental data for LLE (Stephenson, 1993). The range of absorber temperatures is indicated by the gray shaded area. This figure is an adaptation of Figure 11(b) in Perdomo et al. (2021).

is designed to examine whether there exist operating conditions in the absorber such that the solvent mixture remains in a homogeneous liquid phase. Many amine-water and amine-water-CO2 mixtures exhibit partial miscibility and this has in fact enabled the consideration of biphasic solvents (also known as phase-change solvents) as alternatives to conventional solvents (Zhang et al., 2019). Such solvents undergo liquid-liquid phase separation upon heating or CO2 absorption, so that the solvent mixture splits into an amine-rich phase with a high concentration of CO2 and a water-rich phase with a low concentration of CO<sub>2</sub>. Because only the CO<sub>2</sub>-rich liquid phase is sent to the desorber for solvent regeneration, this reduces the energy requirements and equipment costs (Zhang et al., 2019; Papadopoulos et al., 2021). Nevertheless, the aqueous solvent must form a homogeneous liquid phase at the absorber operating conditions for successful operation. Although the process flowsheet configuration considered here does not allow for phase-change solvents, Test 2 can equally be applied to standard (homogeneous) solvents and to phase-change solvents.

In Test 2, we make use of the fact that the solvent mixtures will typically contain a higher mole fraction of water, so that when two liquid phases exist, the properties of the amine-lean liquid phase are of interest. Test 2 can be understood by considering the case of triethylamine (TEA). The predicted phase diagram of aqueous solutions of TEA at 0.101 MPa is shown in Fig. 3 together with the available experimental data (Stephenson, 1993). At typical absorber operating conditions (313 K-333 K), the system exhibits a large LLE region. For this solvent, the homogeneous amine-lean liquid phase is characterized by very low TEA mole fractions, with maximum mole fraction values of TEA of the order of  $10^{-3}$ . Such a low amine concentration would severely limit the achievable CO2 loading and renders this solvent unsuitable. In Test 2, we thus seek to determine whether the solvent mixture exhibits LLE at the absorber conditions and where the boundary of the LLE region lies on the amine-lean side. The resulting maximum amine concentration is tested against a threshold value.

Thus Test 2 consists in determining whether the highest solvent mass fraction  $W^*_{\mathrm{solvent}}(T_{N_a}, P_{N_a}, \mathbf{n})$  at which only one liquid phase can form is above a given threshold value for the given absorber pressure,  $P_{N_a}$ , and temperature,  $T_{N_a}$ . For a mixture of amine and water,  $W^*_{\mathrm{solvent}}(T_{N_a}, P_{N_a}, \mathbf{z}(\mathbf{n}))$  can be calculated by maximizing the solvent mass fraction at which an isobaric–isothermal flash (PT flash) calculation returns a single liquid phase. The PT flash is carried out at  $P_{N_a}$  and the highest allowable absorber temperature. In formulating the

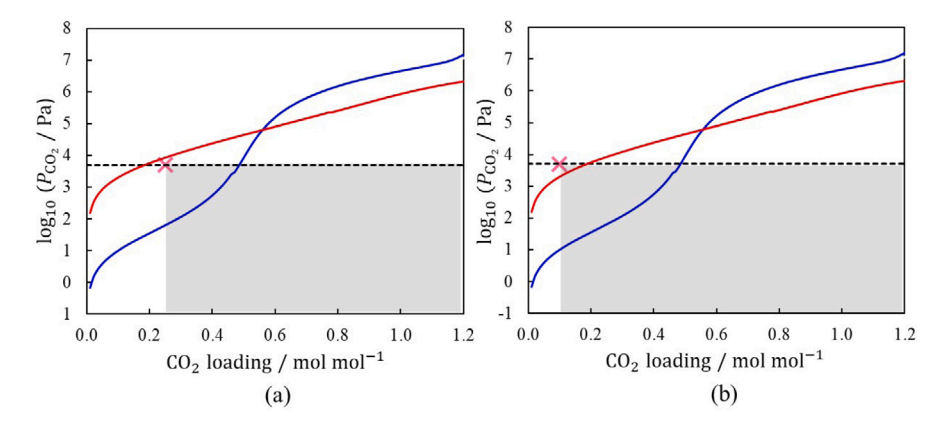


**Fig. 4.** Predicted solubility of CO<sub>2</sub>, expressed as the partial pressure of CO<sub>2</sub> ( $P_{\text{CO}_2}$ ) as a function of the CO<sub>2</sub> loading, in aqueous solutions of MEA (blue continuous curve) and MDEA (red continuous curve) at 30 wt% and 323.15 K. The magenta marker (×) represents the initial guess of the process conditions for the solution of the process optimization problem, with each subfigure representing a different choice: (a) Initial guess of  $T_0 = 323.15$  K and  $\theta_0 = 0.25$  mol mol<sup>-1</sup>, which is above the maximum solubility of CO<sub>2</sub> for MDEA; (b) Initial guess of  $T_0 = 323.15$  K and  $\theta_0 = 0.1$  mol mol<sup>-1</sup>, at which both MEA and MDEA can achieve positive cyclic capacity. The black dashed line indicates a CO<sub>2</sub> partial pressure of 5000 Pa, which is assumed to be the maximum allowable partial pressure  $P_{\text{CO}_2}$  in the flue gas stream. The gray shaded area represents the region of possible values of  $P_{\text{CO}_2}$  and CO<sub>2</sub> loading in the absorber given the initial guess ( $\theta_0$ ). To have a feasible cyclic capacity, the predicted solubility line must intersect the gray rectangular area.

Test 2 optimization problem (as well as subsequent tests), we assume a general PT flash solver is available.

Test 2 is expressed as the following optimization problem:

where  $\hat{x}$  is a vector of variables defined as  $\hat{x} = [z, y, x_{\beta}, x_{\gamma}, \alpha]$  $\beta$ ,  $\gamma$ ,  $W_{\text{solvent}}]^{\mathsf{T}}$ , z is the total composition, y,  $x_{\beta}$  and  $x_{\gamma}$  are the mole fractions in the vapor, first liquid and second liquid phases at equilibrium, respectively,  $\alpha$ ,  $\beta$  and  $\gamma$  are the phase fractions of the vapor, first liquid and second liquid phases at equilibrium, with  $\beta \ge \gamma$ , without loss of generality, NC' is the set of components considered in Test 2, i.e., NC' ={solvent,  $H_2O$ }, and  $MW_{H_2O}$  and  $MW_{solvent}$  are the molecular weights of  $\rm H_2O$  and solvent, respectively.  $\boldsymbol{fl}_{ext}$  is an external function that computes the PT flash for a given global composition z, temperature  $T_{N_a}$ , pressure,  $P_{N_a}$  and molecule n and returns values for  $y, x_{\beta}, x_{\gamma}, \alpha, \beta$  and  $\gamma$ .  $\epsilon_{ph}$  is a small strictly positive scalar value introduced to ensure a homogeneous liquid phase is present. Specifically, the phase fraction of the first (most plentiful) liquid phase is set to be greater than  $\epsilon_{\mathrm{ph}}$ , while the phase fractions of the second liquid phase and of the vapor phase are set to be so small as to be negligible. A value of  $\epsilon_{\rm ph} = 10^{-3}$  is typically used.

It is important to note that the starting point for the solution of Test 2 is at the lowest allowable temperature and nearly pure water,  $z_{\rm solvent}=10^{-3}.$  This is to start the optimization from a feasible point, i.e., a homogeneous liquid phase, setting up to the optimizer to remain in the single-phase region until it reaches the amine-lean boundary of the phase envelope. This approach is particularly useful when the solver encounters discontinuities across the transition between the different regions of the phase diagram.

If the optimal solvent mass fraction obtained is less than the user-defined upper bound on the solvent concentration,  $W^U_{
m solvent}$ , i.e., if

$$W_{\text{solvent}}^* \le W_{\text{solvent}}^U,\tag{11}$$

the molecule is discarded from the search space. The upper bound on the solvent concentration in weight fraction is chosen in order to avoid issues with corrosion and foaming tendency.

*Remarks on Test 2.* We note that the presence of  $CO_2$  in the mixture can induce phase separation so that two liquid phases may form at absorber conditions even when the binary solvent mixture exhibits a single stable liquid phase (Zhang et al., 2019). This eventuality is covered by Test 3.

We have also developed and tested an alternative formulation of Test 2 based on the phase behavior of the ternary mixtures. We have also investigated two further formulations of Test 2 that are based on testing for phase stability only, alleviating the need to compute phase equilibria. We have conducted an extensive investigation of the relative performance of these formulations in terms of reliability and CPU tests and have found that the formulation presented here yields the most effective approach. Further details can be found in Lee (2022).

# 3.1.3. Test 3: Absorption capacity

Test 3 is introduced to ensure that the required absorption capacity can be achieved and to eliminate process conditions and/or solvents that do not meet this criterion. In the design of a solvent for CO2 removal, one of the most important properties is cyclic capacity, defined as the difference between CO2 solubility in the rich solvent and that in the lean solvent. The cyclic capacity determines the solvent circulation rate in the process; a high cyclic capacity often leads to a smaller solvent circulation rate, consequently reducing the equipment size and heat requirement for regeneration. For a given solvent, the cyclic capacity is a function of the design variables, i.e., the lean loading, the temperature of the recycled solvent, and the absorber and desorber operating conditions. The optimal values of these variables can be determined by optimizing the entire process. However, the feasible ranges of these design variables change depending on the solvent structure, making it difficult to provide a good initial guess and even causing failure of the solver to converge. For example, MEA may exhibit higher CO2 solubility than MDEA at given CO2 partial pressure, solvent concentration and temperature. As can be seen in Fig. 4(a), if an initial guess of lean loading  $\theta_0 = 0.25 \text{ mol mol}^{-1}$  and lean solvent temperature  $T_0 = 323.15$ K which is suitable for MEA is adopted for MDEA, it may lead to numerical failure during the optimization as this choice is incompatible with the maximum CO2 solubility in MDEA. Indeed, the maximum solubility of CO<sub>2</sub> for MDEA at 323.15 K is 0.1 mol mol<sup>-1</sup> as shown in Fig. 4(b), where the possible range of partial pressures of CO<sub>2</sub> in the absorber at 323.15 K is denoted by a gray box.

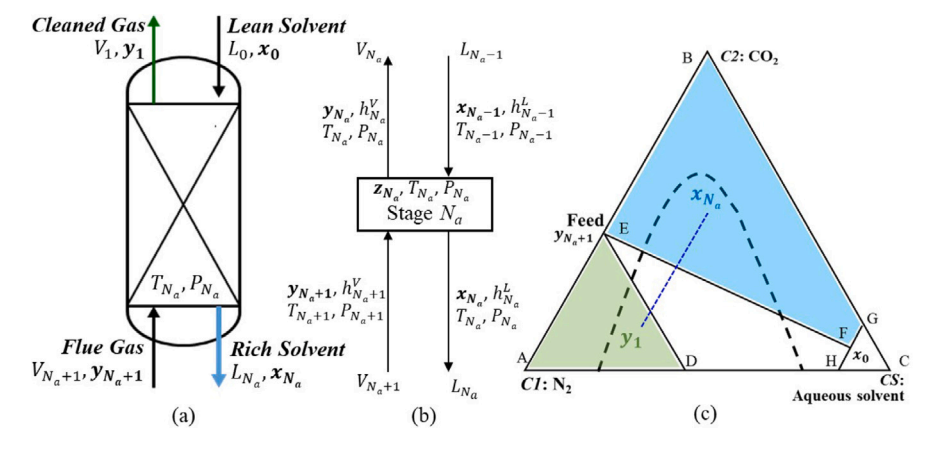


Fig. 5. Schematic of (a) the absorber envelope, (b) the last equilibrium stage of the absorber and (c) a fixed temperature and pressure ternary phase diagram of C1 ( $N_2$ ), C2 ( $CO_2$ ), and CS (aqueous solvent solution) at  $T_{N_a}$ ,  $P_{N_a}$ . The region of acceptable clean gas mole fractions  $\mathbf{y}_1$  is denoted by the green shaded triangle EAD and the region of desirable rich solvent mole fraction vectors  $\mathbf{x}_{N_a}$  is denoted by the blue shaded area BEFG. The solid line  $\overline{[\mathbf{y}_{N_a+1},\mathbf{x}_0]}$  represents the mixing line of the feed streams on the ternary diagram. The thick dashed curve represents the vapor-liquid phase boundary. Note that  $\mathbf{x}_{N_a}$  represents the mole fraction vector of the single liquid phase that is desired in the absorber.

The desired purity of clean gas is not achievable when  $\theta_0$  is set above the maximum solubility of  $\mathrm{CO}_2$ , and this may cause numerical failure in the absorber. To avoid combinations of the operating conditions that lead to an unphysically high  $\mathrm{CO}_2$  loading, Test 3 is used to identify the upper and lower bounds on the lean-solvent loading  $(\theta_0)$  based on the thermodynamic feasibility of separation on the bottom stages of the absorber and desorber, respectively. We first describe how to compute the desired bounds and then show their use within Test 3.

Absorber. The purpose of Test 3 is akin to that suggested by Gopinath (2017) in the context of physical gas absorption. The formulation of Gopinath (2017) was developed for ternary mixtures to determine whether target  $CO_2$  removal can be achieved with a given solvent, by maximizing the absorber pressures with respect to the global composition, temperature and pressure on the last stage of the absorber. Here, it is adapted to take into account quaternary mixtures of  $N_2$ ,  $CO_2$ , amine solvent, and water, and their VLLE, by assuming that the ratio of water to solvent remains unchanged through the absorber, allowing the aqueous solvent mixture (water+solvent) to be lumped into one hypothetical component, CS, so that the mixture considered can be treated as a pseudo-ternary mixture.

To develop the formulation for Test 3, we consider three feasibility conditions: the coexistence of two phases (vapor and liquid) at the bottom stage of the absorber; the thermodynamic feasibility of the desired purity in the clean gas stream; and the capacity of the solvent to achieve positive cyclic capacity. We show the mathematical representation of each constraint before combining them into an optimization formulation.

The coexistence of a vapor phase and a homogeneous liquid phase in stage  $N_a$  of the absorber must be ensured to avoid any discontinuities caused by having only one phase or two liquid phases in this stage during process optimization. This condition is expressed by the following constraints, which are similar to those used in Test 2 for the binary solvent mixture:

$$\begin{split} & f I_{ext} \left( \boldsymbol{z}_{N_a}, T_{N_a}, \boldsymbol{y}_{N_a}, \boldsymbol{x}_{\beta, N_a}, \boldsymbol{x}_{\gamma, N_a}, \alpha, \beta, \gamma, P_{N_a}, \boldsymbol{n} \right) = 0 \\ & \alpha \geq \epsilon_{\text{ph}} \\ & \beta \geq \epsilon_{\text{ph}} \\ & \gamma \leq \epsilon_{\text{ph}} \end{split} \tag{12}$$

Next, it is necessary to derive a constraint that enforces separation feasibility. Here, we adapt the formulation in Gopinath (2017) to the context of a  $\mathrm{CO}_2$  chemical absorption process. Consider the compositions and flowrates of the streams entering and leaving the absorber

envelope as described in Figs. 5(a) and (b). The assumptions used for the derivation are as follows:

- 1. The number of moles of solvent lost to the vapor stream over the length of column is less than the number of moles transferred from the gas stream to the liquid stream, i.e.,  $L_{N_a} > L_0$ .
- 2. The concentrations of two of the components  $N_2$  and  $CO_2$  in the vapor feed stream entering the absorber are greater than the concentrations of those components in the lean solvent stream entering the top of the column. That is,  $y_{N_a+1,N_2} \geq x_{0,N_2}$  and  $y_{N_a+1,CO_2} \geq x_{0,CO_2}$ .
- 3. Since the column operation aims at separating the impurity  $(CO_2)$  from the feed stream, the treated clean gas stream leaving the top of the column must be enriched in  $N_2$ , i.e.,  $y_{1,N_2} > y_{N_a+1,N_2}$ .

The feasible regions for the separation are shown in a ternary diagram in Fig. 5(c). Region AED represents the target compositions  $\mathbf{y}_1$ , while region BEFG indicates all possible compositions  $\mathbf{x}_{N_a}$  of the rich solvent. The separation is feasible when the vapor–liquid boundary (black dashed curve) at  $T_{N_a}$ ,  $P_{N_a}$  intersects the region BEFG. Given the feed mixing line  $\overline{[\mathbf{y}_{N_a+1},\mathbf{x}_0]}$ , the line segment  $\overline{[\mathbf{y}_1,\mathbf{x}_{N_a}]}$  (blue dashed line) must intersect the mixing line to satisfy the overall material balance.

An analytical equation can be derived to represent this condition using the equations of the two line segments and their slopes, in addition to the overall and component material balances. The resulting constraint is given by:

$$x_{N_a,\text{CO}_2} - y_{N_a+1,\text{CO}_2} - \frac{\left(y_{N_a+1,\text{CO}_2} - x_{0,\text{CO}_2}\right)}{\left(y_{N_a+1,\text{N}_2} - x_{0,\text{N}_2}\right)} \left(x_{N_a,\text{N}_2} - y_{N_a+1,\text{N}_2}\right) \ge \epsilon_{\text{sp}},$$
(13)

where  $x_{N_a,N_2}$  and  $x_{N_a,CO_2}$  are the liquid mole fractions of components  $N_2$  and  $CO_2$  in the stream leaving the last (bottom) stage of the absorber,  $x_{0,N_2}$  and  $x_{0,CO_2}$  are the equilibrium liquid mole fractions of components  $N_2$  and  $CO_2$  of the lean solvent stream entering the top of the absorber and  $y_{N_a+1,N_2}$  and  $y_{N_a+1,CO_2}$  are the gas mole fractions of components  $N_2$  and  $CO_2$  of the stream entering the bottom of absorber, i.e, the flue gas. Note that the total composition of flue gas,  $y_{N_a+1}$ , is usually given and the total composition of the liquid stream at the last stage of absorber,  $x_{N_a}$ , is obtained by calculating the phase equilibrium for a fixed  $z_{N_a}$ ,  $T_{N_a}$  and  $P_{N_a}$ . For a comprehensive description of the

derivation and assumptions used, the reader is referred to Gopinath (2017) and section 3.2.3.2 therein.

Finally, a feasible solvent must have a positive cyclic capacity and this restricts the allowable values of the lean loading  $\theta_0$ . This can be expressed as:

$$\frac{x_{N_a, \text{CO}_2}}{x_{N_a, \text{solvent}}} - \theta_0 \ge \epsilon_{\text{cyclic}},\tag{14}$$

where  $\epsilon_{\text{cyclic}}$  is a strictly positive number. Combining the three conditions (12), (13) and (14), the upper bound on the solvent loading is given as a result of the following optimization problem:

$$\begin{aligned} \theta_0^U(\bar{\mathbf{x}},P_{N_a},\mathbf{n}) &= \max_{\bar{\mathbf{x}} \in \bar{X}} \quad \theta_0 \\ \text{s.t.} \quad fl_{ext}\left(\mathbf{z}_{N_a},T_{N_a},\mathbf{y}_{N_a},\mathbf{x}_{\beta,N_a},\mathbf{x}_{\gamma,N_a},\alpha,\beta,\gamma,P_{N_a},\mathbf{n}\right) &= 0 \\ & \alpha \geq \epsilon_{\text{ph}} \\ & \beta \geq \epsilon_{\text{ph}} \\ & \frac{x_{\beta,N_a,\text{CO}_1}}{x_{\beta,N_a,\text{solvent}}} - \theta_0 \geq \epsilon_{\text{cyclic}} \\ & x_{\beta,N_a,\text{cO}_2} - y_{N_a+1,\text{CO}_2} - \frac{\left(y_{N_a+1,\text{CO}_2} - x_{0,\text{CO}_2}\right)}{\left(y_{N_a+1,N_2} - x_{0,N_2}\right)} \\ & \times \left(x_{\beta,N_a,N_2} - y_{N_a+1,N_2}\right) \geq \epsilon_{\text{sp}} \\ & \sum_{i=1}^{NC} z_{N_a,i} &= 1 \\ & 0 \leq z_{N_a,i} \leq 1 \quad \forall i \in NC \\ & \max\left(T_{\text{mp}}\left(\mathbf{n}\right) + 10, T_{\text{op}}^L\right) \leq T_{N_a} \leq T_{\text{op}}^U \end{aligned} \tag{15}$$

where  $\tilde{\mathbf{x}}$  is a vector of variables defined as  $\tilde{\mathbf{x}} = [\mathbf{z}_{N_a}, T_{N_a}, \theta_0, \mathbf{y}_{N_a}, \mathbf{x}_{\beta,N_a}, \mathbf{x}_{\gamma,N_a}, \alpha, \beta, \gamma]^\mathsf{T}$ ,  $\tilde{X}$  is a nonempty compact set, and NC is the set of components in the system, i.e.,  $NC = \{N_2, CO_2, H_2O, \text{ solvent}\}$ .

Desorber. A lower bound on the lean loading  $\theta_0$  can be obtained in a similar fashion, by determining the minimum loading achievable at the bottom stage of the desorber with respect to the global composition  $\mathbf{z}_{N_d}$  and the temperature  $T_{N_d}$  at the minimum allowable operating pressure  $P_{N_d}^L$ . Since a lower content of solvent in the system leads to a lower amount of  $\mathrm{CO}_2$  absorbed, the search for the feasible bound may converge to a trivial solution, where the liquid stream from the bottom of the absorber is almost pure water. To ensure that the solvent concentration in the rich solvent liquid stream is greater than the minimum required solvent concentration, the following constraint is used:

$$\frac{x_{N_d,\text{solvent}}}{x_{N_d,\text{solvent}} + x_{N_d,\text{H}_2\text{O}}} - \frac{x_{N_d,\text{solvent}}}{x_{N_d,\text{solvent}} + x_{N_d,\text{H}_2\text{O}}} \ge \epsilon_{\text{sol}},\tag{16}$$

where  $x_{N_d, \text{solvent}}, x_{N_d, \text{H}_2\text{O}}$  are the liquid solvent and H<sub>2</sub>O mole fractions in the lean solvent stream leaving the desorber, and  $\epsilon_{\text{sol}}$  is a strictly positive number.

The resulting optimization problem for the lower bound of the lean loading is given as follows:

$$\begin{split} \theta_0^L(\bar{\mathbf{x}}, P_{N_d}, \mathbf{n}) &= \min_{\bar{\mathbf{x}} \in \bar{X}} & \theta_0' \\ \text{s.t.} & f I_{ext} \left( z_{N_d}, T_{N_d}, \mathbf{y}_{N_d}, \mathbf{x}_{\beta, N_d}, \mathbf{x}_{\gamma, N_d}, \alpha, \beta, \gamma, P_{N_d}, \mathbf{n} \right) = 0 \\ & \alpha \geq \epsilon_{\text{ph}} \\ & \beta \geq \epsilon_{\text{ph}} \\ & \gamma \leq \epsilon_{\text{ph}} \\ & \theta_0' = \frac{x_{\beta, N_d, \text{CO}_2}}{x_{\beta, N_d, \text{solvent}}} \\ & \frac{x_{\beta, N_d, \text{solvent}}}{x_{\beta, N_d, \text{solvent}} + x_{\beta, N_d, H, Q}} - \frac{x_{\beta, N_d, \text{solvent}}}{x_{\beta, N_d, \text{solvent}} + x_{\beta, N_d, H, Q}} \geq \epsilon_{\text{sol}} \\ & 0 \leq z_{N_d, i} \leq 1 \quad \forall i \in NC \\ & \sum_{i=1}^{NC} z_{N_d, i} = 1 \\ & \max \left( T_{\text{mp}} \left( \mathbf{n} \right) + 10, T_{\text{op}}^L \right) \leq T_{N_d} \leq T_{\text{op}}^U \end{split}$$

where  $\theta_0'$  is a lean loading calculated from the liquid composition at the bottom of the desorber,  $\bar{x}$  is a vector of variables  $\bar{x} = [z_{N_d}, T_{N_d}, \theta_0', y, x_{\beta, N_d}, x_{\gamma, N_s}, \alpha, \beta, \gamma]^{\mathsf{T}}$  and  $\bar{X}$  is a nonempty compact set.

Test 3. If the new lower bound on the lean loading is larger than the upper bound (i.e.,  $\theta_0^U < \theta_0^L$ ) or if problem (15) or (17) is infeasible (i.e., no feasible upper or lower bound on the lean loading is identified), it is clear that no process conditions will be feasible for CO<sub>2</sub> absorption, and the current solvent structure  $\boldsymbol{n}$  is eliminated from the search space. Otherwise, the solution of Test 3 is used to provide a reduced range for the loading  $[\theta_0^L, \theta_0^U]$ , for use in the primal problem. Furthermore, the initial guess on  $\theta_0$  is updated, for example to  $\theta_0^L$ , if the default value is not within the feasible ranges of  $[\theta_0^L, \theta_0^U]$ , in order to prevent numerical difficulties.

# 3.1.4. Test 4: desorber operating pressure range

Once an updated lean loading range  $[\theta_0^1, \theta_0^U]$  has been generated from Test 3, Test 4 is used to tighten the upper bound on the desorber pressure,  $P_{N_d}$ . The upper bound is given by the highest pressure at which: 1) vapor–liquid equilibrium occurs on the bottom stage of the desorber, and 2) there exists a lean solvent composition that falls within the target lean loading range. An additional constraint on the solvent weight fraction in the stream leaving the bottom stage of the absorber  $(W_{N_d})$  is imposed in order to prevent the optimization algorithm from converging to a trivial solution. Here, we assume that only trace amounts of  $N_2$  can be present so that  $N_2$  can be neglected. The resulting formulation is as follows:

$$\begin{split} P_{N_d}^U(\check{\mathbf{x}}, \mathbf{n}) &= \max_{\check{\mathbf{x}} \in \check{X}} \quad P_{N_d} \\ \text{s.t.} \quad fl_{ext} \left( z_{N_d}, T_{N_d}, P_{N_d}, \mathbf{y}_{N_d}, \mathbf{x}_{\beta, N_d}, \mathbf{x}_{\gamma, N_d}, \alpha, \beta, \gamma, \mathbf{n} \right) = 0 \\ \alpha &\geq \epsilon_{\text{ph}} \\ \beta &\geq \epsilon_{\text{ph}} \\ \gamma &\leq \epsilon_{\text{ph}} \\ \frac{x_{\beta, N_d, \text{solvent}}}{x_{\beta, N_d, \text{solvent}}} - \frac{x_{N_d, \text{solvent}}}{x_{N_d, \text{solvent}} + x_{N_d, \text{H2O}}} \geq \epsilon_{\text{sol}} \\ \theta_0' &= \frac{x_{\beta, N_d, \text{col2}}}{x_{\beta, N_d, \text{solvent}}} \\ W_{N_d} &\geq W_{0, \text{solvent}} \\ W_{N_d} &= \frac{x_{\beta, N_d, \text{solvent}} MW_{\text{solvent}}}{x_{\beta, N_d, \text{solvent}} MW_{\text{solvent}}} \\ W_{N_d} &= \frac{x_{\beta, N_d, \text{solvent}}}{x_{\beta, N_d, \text{solvent}} MW_{\text{solvent}}} \\ 0 &\leq z_{N_d, i} \leq 1 \quad \forall i \in NC \\ \max \left( T_{\text{mp}} \left( \mathbf{n} \right) + 10, T_{N_d}^L \right) \leq T_{N_d} \leq T_{\text{op}}^U \\ \theta_0^L \leq \theta_0' \leq \theta_0^U \\ \sum_{i=1}^{N_C} z_{N_d, i} = 1 \end{split}$$

where  $\check{\mathbf{x}}$  is a vector of variables defined as  $\check{\mathbf{x}} = [\mathbf{z}_{N_d}, T_{N_d}, \theta_0', \mathbf{y}_{N_d}, \mathbf{x}_{\beta, N_d}, \mathbf{x}_{\beta, N_d}, \alpha, \beta, \gamma]^\mathsf{T}$ , and  $\check{X}$  is a nonempty compact set.

(18)

# 4. Optimization strategy and implementation

Following the development of feasibility tests for absorption—desorption processes using binary solvents, these can be integrated within an overall CAMPD framework. The optimization strategy and implementation are discussed in this section, before their application to CO<sub>2</sub> capture process design.

### 4.1. Algorithm overview

An overview of the algorithm is provided in Fig. 6. It follows a standard outer approximation framework (Duran and Grossmann, 1986; Kocis and Grossmann, 1989; Viswanathan and Grossmann, 1990) with the addition of feasibility tests as precursors to the solution of the primal problem.

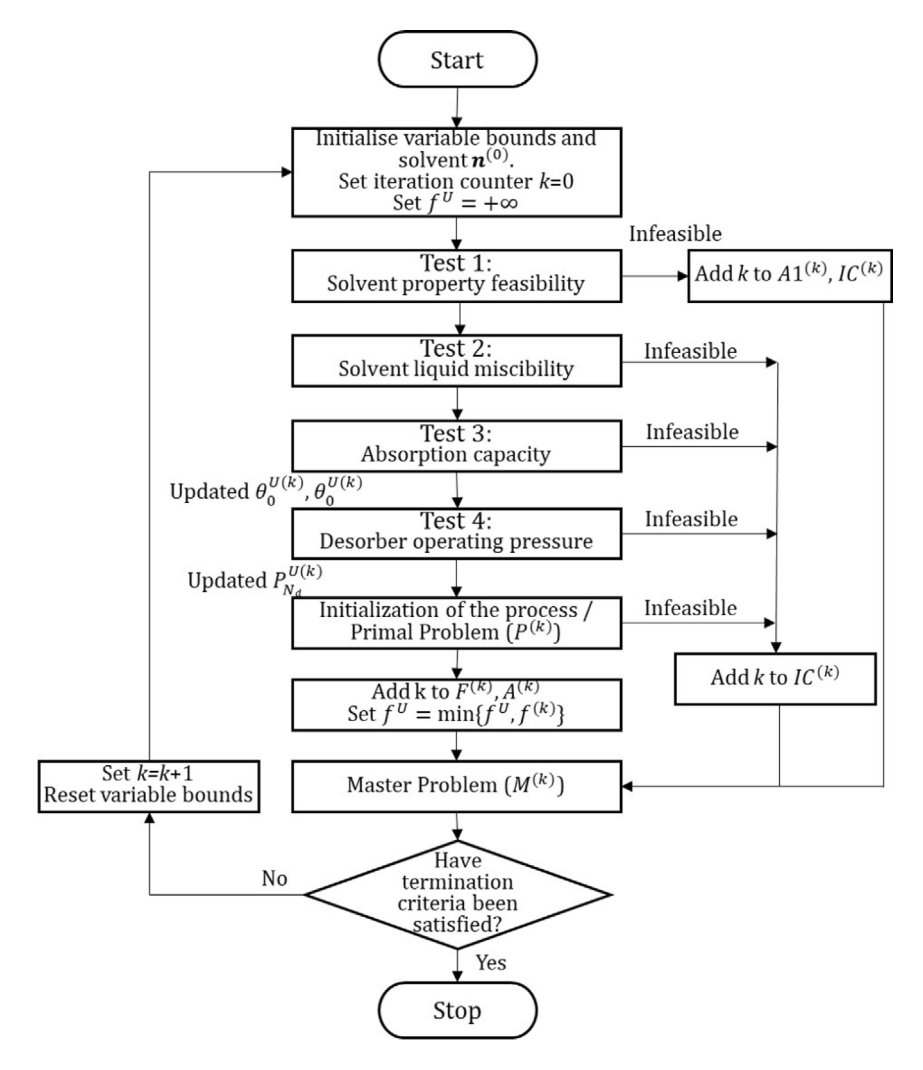


Fig. 6. An overview of the proposed CAMPD algorithm.

An alternating finite sequence of NLP subproblems and MILP subproblems are solved. Given the feasible domain defined with tightened bounds on the operating conditions from Tests 3 and 4, the primal problem of the OA algorithm is formulated as a nonlinear process optimization problem over continuous variables with fixed solvent structure (see Problem  $P^{(k)}$  in the Supplementary Information).

The master problem is formulated by deriving a set of linearized constraints and objective functions (hyperplanes) from the solution of each primal problem, such that the original problem domain is approximated via a polyhedral representation. As iterations proceed, the approximation is improved by accumulating the linearized equations and tightening the outer bounds on the feasible region of the problem. The final form of the master problem differs depending on the outcome of the feasibility tests and of the primal problem, which determines what linearizations are included in the problem.

In the original OA, if the primal is infeasible at iteration k (Duran and Grossmann, 1986), an alternative "infeasible" primal problem is solved and added to the master problem. Given that it is difficult to find a feasible solution to the infeasible primal problem for highly nonconvex MINLPs (Grossmann et al., 2002), the solution of the infeasible primal is not included in this study. Instead, the integer variables that lead to an infeasible primal are excluded by adding an integer cut (see Supplementary Information) to the master problem. It should noted that no failure in solving the primal problem is encountered in the

case studies, thanks to the robustness of the proposed algorithm where infeasible combinations of molecular structure and process conditions are discarded by solving the feasibility tests.

### 4.2. Termination criteria

When using the OA with augmented penalty (AP) framework to overcome the nonconvexities of the problem, care must be taken in choosing a termination criterion to prevent the algorithm from converging to a solution prematurely. For a convex MINLP, the master problem produces a valid lower bound on the objective function of the primal problem and this lower bound increases monotonically as iterations proceed, while updates of the upper bound on the problem are generated through the primal problem. The best NLP solution found can thus be guaranteed to be the global optimum (assuming there are no numerical failures of the NLP solver) when the lower bound exceeds or is close to the upper bound for the convex MINLP. However, using such a criterion as a stopping rule for nonconvex MINLP problems may result in premature convergence, particularly when the set of linear approximations leads to part of the feasible region being cut off, possibly eliminating a global solution (Floudas, 1995). It therefore becomes necessary to employ heuristics to improve the quality of the solutions. Generally good convergence behavior has been observed using the stopping criteria presented in Bowskill et al. (2020). Hence,

Table 3 Key input parameters and specifications for the  ${\rm CO_2}$  capture case study and the application of the feasibility tests.

Parameter	Symbol	Value
Degree of CO <sub>2</sub> captured (%)	_	90
Condenser temperature (K)	$T_{N_{\star}}^{L}$	333
Absorber temperature in Test 1 (K)	$T_{N_a}$	323
Absorber operating pressure (MPa)	$P_{N_a}$	0.1
Weight fraction of amine solvent (kg kg <sup>-1</sup> )	$W_{0, m solvent}$	0.304
Min. approach temperature (K)	$\Delta T_{\min}$	10
Initial bounds on desorber pressure (MPa)	$[P_{N_d}^L, P_{N_d}^U]$	[0.1, 5]
Initial bounds on handling temperature (K)	$[T_{\mathrm{sh}}^L, T_{\mathrm{sh}}^U]$	[303, 333]
Initial bounds on lean solvent temperature (K)	$[T_0^{L}, T_0^{U}]$	[313, 353]
Initial bounds on lean loading (mol mol <sup>-1</sup> )	$[ heta_0^L, heta_0^U]$	[0.02, 2]
Minimum operating temperature (K)	$T_{ m op}^L$	313
Upper bound on the solvent concentration (kg kg <sup>-1</sup> )	$W_{ m solvent}^U$	0.5
Phase fraction parameter	$\epsilon_{ m ph}$	$1 \times 10^{-3}$
Separation feasibility parameter	$\epsilon_{ m sp}$	$1 \times 10^{-3}$
Minimum allowable cyclic capacity	$\epsilon_{ m cyclic}$	$1 \times 10^{-1}$
Minimum allowable solvent loss	$\epsilon_{ m sol}$	$5 \times 10^{-2}$

we resort to termination based on the same heuristics by which the algorithm is stopped when: (1) the number of iterations at which the augmented penalty term becomes nonzero exceeds a pre-defined limit,  $N_{\rm max,slack}$ , (2) the number of unique molecules that has been evaluated either in the feasibility tests or the primal problem exceeds a pre-defined limit  $N_{\rm max,unq}$ , and 3) when the MILP master problem becomes infeasible

### 4.3. Implementation and case study

An automated implementation of the proposed CAMPD algorithm is developed in C++ in Visual Studio 2019, with an interface to gPROMS ModelBuilder 7.0.7 (Process Systems Engineering, 1997-2022) using gO:RUN functionality and an interface to the Gurobi 8.1 MILP (Gurobi Optimization, LLC, 2022). The feasibility tests are implemented in FORTRAN and gPROMS ModelBuilder. The results of the tests, such as the updated bounds and infeasibility of the molecule, are transferred to the primal problem via the gO:RUN interface. The default continuous nonlinear optimizer in gPROMS, which makes use of a sequential quadratic programming (SQP) method, is applied to solve the primal problems. The gradients of the objective function and active inequality constraints are calculated using first-order forward finite differences with respect to integer variables and central differences for the continuous variables. All computations were run on single Intel(R) Xeon(R) Gold 5122 CPU @ 3.60 GHz processor with 384 GB of RAM.

CO2 capture from an exhaust gas generated by a 400 MWe CCGT power plant (Alhajaj et al., 2016), as described in Section 2.2, is considered as a case study to assess the performance of the proposed feasibility tests and the proposed CAMPD framework. The key input parameters and the pre-specified bounds on the design variables that are used throughout the study are provided in Table 3. The lower bounds and upper bounds for Test 1 are listed in Table 2. To investigate the impact of the feasibility tests, the reduced solvent design space is considered and the results are summarized in Section 5.1, followed by the results obtained by applying the proposed algorithm to the full CAMPD problems in Sections 5.2-5.5. For each feasibility test, the solution of PT flash calculations ( $fl_{ext}$ ) is an essential step to ensure fluid mixtures exhibit the desired fluid phase behavior. From the analysis of the performance of PT flash approaches in Lee (2022), it appears that the HELD algorithm proposed by Pereira et al. (2012) is particularly well suited to the analysis of systems with complex phase behavior such as the ones considered here. In principle, the use of the HELD algorithm is advantageous because the PT flash problem is formulated in the space of temperature, volume and mole numbers, which are natural variables for the SAFT- $\gamma$  Mie EOS, thereby avoiding the use of a pressure solver. This is confirmed in practice, and the

algorithm is found to be robust and reliable in the identification of the types of phase, phase compositions, and phase fractions that correspond to the best-known or global minimum of the Gibbs free energy within a practical computational time. Another option is to use the general PT flash calculation framework embedded in the gPROMS ModelBuilder 7.0.7 software package, which we have found to provide faster computations, at a cost of a small loss in reliability. In view of this, we use both approaches in assessing the performance of the feasibility tests in which the entire set of feasible solvents is enumerated: the HELD algorithm is introduced for Test 2, which is most challenging, and the gPROMS PT flash algorithm is utilized in Tests 3 and 4 to manage the computational costs. We use the HELD algorithm in the solution of all feasibility tests when solving CAMPD problems as a much smaller number of molecules is evaluated.

### 5. Results

# 5.1. Performance of the feasibility tests: Application to selected solvent space

An evaluation of the entire space of possible solvents is firstly carried out to assess the performance of the proposed feasibility tests. For the purpose of analysis, the set of all possible combinations of solvent candidates is generated in accordance with the molecular feasibility constraints provided in Eqs. (2)–(8) with the bounds of  $n_{\rm OH}^U=2$ ,  $n_{G_A}^L=1$ ,  $n_{G_A}^U=2$  and  $n_{\rm iso}^U=5$ , so that small amines and diamines functionalized by up to two hydroxyl groups are generated. The number of each functional groups i is limited by the bounds  $n_i^L=0$ ,  $n_i^U=10$ ,  $i=1,\ldots,N$ . These define a molecular design space of 4179 possible solvent structures. The investigation of the effectiveness of the feasibility tests is carried out by a brute-force search on the entire design space.

The overall results of applying the feasibility tests to the specifications in Table 3 are summarized in Table 4 and Figs. 7 and 8. Within the 4179 candidate molecules, only 1450 solvents pass all feasibility tests. As can be seen in Table 4, the majority of the alkylamines are found to be infeasible in Test 1 and Test 2, mainly due to their low water miscibility as well as their low safety and environmental performance. For instance, triethylamine (TEA) is eliminated by Test 2 due to its low water miscibility, as seen previously in Fig. 3. The maximum mass fraction ( $W^*_{T_{N_a},P_{N_a},\mathrm{solvent}}$ ) of TEA that can ensure a homogeneous liquid phase at absorber operating conditions is calculated with SAFT- $\gamma$  Mie to be 0.019 in mass fraction (0.0015 in mole fraction). This indicates that the constraint  $W^U_{\mathrm{solvent}}$  (= 0.5)  $\leq W^*_{\mathrm{solvent}}$  is violated and TEA should be eliminated from the molecular design space.

The performance of Tests 3 and 4 is examined for those solvents that pass Tests 1 and 2. Tests 3 and 4 lead to tighter bounds on the lean loading and desorber pressure, as shown by the percentage deviation, and the average values of the updated bounds, presented in the Table 4. As can be seen, there is a significant improvement in the average value of the updated bounds, suggesting that many infeasible process conditions can be removed by the feasibility tests. The large deviations in the maximum lean loading and desorber pressure indicate that providing a universal initial guess that is feasible for all solvent molecular structures is very difficult. It is therefore important to provide a systematic way to recognize the feasible combinations of process conditions and solvents. Similar trends can be seen in Fig. 7, in which density plots of the normalized values of the bounds obtained from the feasibility tests are displayed, together with the minimum, maximum, median, and interquartile ranges. To produce the plots, each bound has been normalized using the minimum and maximum values of the ranges obtained as follows:

$$\bar{p}_{n,q} = \frac{p_{n,q} - \min_{n} p_{n,q}}{\max_{n} p_{n,q} - \min_{n} p_{n,q}}$$
(19)

where  $\bar{p}_{n,q}$  is a normalized bound value for the molecule n and bound q where  $q \in \{\theta_0^L, \theta_0^U, P_{N_d}^U\}$  and  $p_{n,q}$  is an updated bound for n and

**Table 4**Overall results of feasibility tests over the complete list of 4179 candidate molecules, broken down by molecular class. The initial values of the bounds are  $\theta_0^L = 0.02$  mol mol<sup>-1</sup>,  $\theta_0^U = 2$  mol mol<sup>-1</sup>,  $P_N^U = 5$  MPa.

	Total	Mono Amine		Diamine	
		Alkanol-	Alkyl-	Alkanol-	Alkyl-
Number of molecules tested	4179	765	416	1918	1080
Number of molecules eliminated by Test 1	791	64	292	30	405
Number of molecules eliminated by Test 2	821	292	124	341	64
Number of molecules eliminated by Test 3	1109	124	0	430	555
Number of molecules eliminated by Test 4	8	0	0	6	2
Number of feasible molecules	1450	285	0	1111	54
Percentage deviation of $\theta_0^L$	1.12	1.17	_	1.08	0.12
Percentage deviation of $\theta_0^U$	22.52	7.81	_	13.18	3.44
Percentage deviation of $P_N^U$	2.15	3.41	-	1.42	0.95
Average value of updated bound, $\theta_0^L$ (mol mol <sup>-1</sup> )	0.0382	0.0330	-	0.0391	0.0484
Average value of updated bound, $\theta_0^U$ (mol mol <sup>-1</sup> )	0.7283	0.3480	-	0.8178	0.9612
Average value of updated bound, $P_{N_d}^U$ (MPa)	0.3427	0.3601	-	0.3383	0.3424

**Table 5**Values of the optimization variables for five starting points, S1–S5, used for the solution of the primal problem for MEA and AMPD.

Variable	S1	S2	S3	S4	S5
Lean loading, $\theta_0$ (mol mol <sup>-1</sup> )	0.10	0.20	0.30	0.40	0.50
Lean solvent temperature, $T_0$ (K)	313.15	333.15	323.15	323.15	313.15
Desorber pressure, $P_{N_d}$ (MPa)	0.180	0.250	0.150	0.200	0.180

q obtained by solving the feasibility tests. From Fig. 7, it is evident that the distribution of the bounds on each process variable is multimodal. This indicates that the feasible region of process variables considered (solvent lean loading and desorber pressure) is highly dependent upon solvent structure and highlights why identifying an initial feasible combination of process conditions is challenging when many chemically-different solvents are to be evaluated. It emphasizes the importance of developing a robust algorithm that can determine the feasible process domain and good initial guesses of the design variables for each solvent. For the case of MDEA, for example, a more stringent maximum allowable value of lean-solvent loading,  $\theta_0^U = 0.237$ , is set as a result of Test 3. This implies that if the initial guess on the lean loading were set to be greater than 0.237, the initialization of the process model would lead to numerical failure, making it impossible to evaluate the performance of this solvent.

Five hundred process simulations for randomly generated combinations of the lean loading, desorber pressure, and lean solvent temperature are performed for 2-(2-aminoethylamino)ethanol (AEEA) and for MEA to illustrate the reduction of the process ranges obtained with the feasibility tests and to explore whether this leads to the exclusion of any feasible points. In Fig. 8, the space of combinations of the process variables,  $\theta_0$ ,  $P_{N_d}$ , and  $T_0$ , is represented as a 3-dimensional spider plot (i.e., triangle), using values normalized with respect to the lower and upper bounds in Table 3. The normalized bounds all cover the range [0, 1], as denoted by the black triangles, and the updated normalized bounds following the feasibility tests are denoted by the red triangles. Combinations of the process variables that fail to converge (Fig. 8(a)) or are infeasible as they violate the design constraints such as the maximum allowable operating temperature,  $T_{\mathrm{op}}^{U}$ , (Fig. 8(b)) are found both within and outside the region defined by the reduced bounds. As can be seen in Fig. 8(c), however, all feasible operating conditions are within the reduced process operating ranges, indicating that the feasibility tests can eliminate some of the infeasible combinations of the process operating conditions systematically without cutting off the potential solutions. For MEA, the feasibility tests yield a particularly good representation of the feasible region obtained with 500 simulations, while more overestimation is observed for AEEA.

To exemplify the impact of the feasibility tests and of the updated bounds on the solution of the primal problem, the specific cases of MEA and 2-amino-2-methyl-1,3-propanediol (AMPD) are investigated.

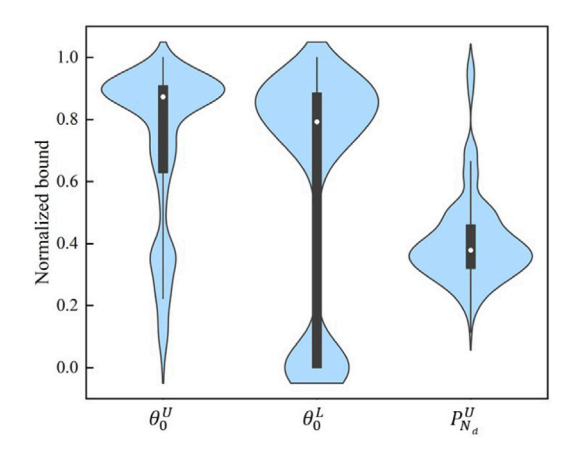


**Fig. 7.** Violin plots with kernel-density estimate displaying the maximum, the minimum, the median, the first and third quartile ranges of the normalized value of each process bounds  $(\theta_0^U, \theta_0^L, P_{N_d}^U)$  for the feasible molecules. The width of each curve corresponds to the approximate frequency of values of the bound in each region.

For each solvent, the primal problem is solved from five starting points distributed within the initial bounds on the design variables in order to investigate the impact of the choice of the initial guess and also to increase the likelihood of identifying a global solution. The five starting points, S1–S5, are given in Table 5. Two algorithmic options, with feasibility and without feasibility tests, are considered for each solvent and the usefulness of the feasibility tests is assessed based on the ability to converge to a solution from each starting point and on the average computational time. Where feasibility tests are used, the values of the starting points are updated automatically if the variable bounds generated as a result of the feasibility tests indicate that they are infeasible for the specified solvent. Specifically, the initial lean loading is set to its new lower bound,  $\theta_0 = \theta_0^L$ , if the original initial value is found to be infeasible. In the same manner, the updated upper bound is assigned to the initial desorber pressure,  $P_{N_d} = P_{N_d}^U$ .

The results of the optimization runs carried out are summarized in Table 6. The average computational cost is calculated only over the CPU times of the successful runs for both algorithmic options, thereby neglecting the cost of failed runs, which can often be large. It can be seen that all 10 runs with feasibility tests converge successfully, while only 5 of the 10 runs converge in the absence of feasibility tests. For MEA, the average computational cost is slightly higher (by 9%) for the runs with feasibility tests. The algorithm without feasibility tests fails to converge for starting points S4 and S5 due to the infeasible value of the lean-solvent loading at the starting point for these runs. The algorithm with the feasibility tests converges for all runs by updating the starting point for the lean-solvent loading after Test 3. The new

Table 6 Outcome of the tests and of the solutions of the primal problem for MEA and AMPD over five runs. The bounds used for the solution of the problem are reported, followed by the optimal objective and variable values and statistics on all the runs. Only the run with the smallest objective function is presented as an optimal solution. The unit of ton-CO<sub>2</sub> is defined as the amount of CO<sub>2</sub> captured from the flue gas in the absorber in metric tons.

MEA		AMPD	
no tests	with tests	no tests	with tests
0.02	0.02	0.02	0.0420
2.0	0.3995	2.0	0.3418
0.80	0.305	0.80	0.340
29.808	29.805	25.735	25.735
9.322	9.321	7.921	7.928
397.18	397.15	398.94	398.94
0.1597	0.1595	0.2132	0.2134
0.4764	0.4764	0.4744	0.4744
0.3168	0.3169	0.2611	0.2610
313.16	313.15	335.44	335.43
0.206	0.206	0.216	0.216
3	5	2	5
251.76	273.91	328.56	294.31
	0.02 2.0 0.80 29.808 9.322 397.18 0.1597 0.4764 0.3168 313.16 0.206	no tests         with tests           0.02         0.02           2.0         0.3995           0.80         0.305           29.808         29.805           9.322         9.321           397.18         397.15           0.1597         0.1595           0.4764         0.4764           0.3168         0.3169           313.16         313.15           0.206         0.206           3         5	no tests         with tests         no tests           0.02         0.02         0.02           2.0         0.3995         2.0           0.80         0.305         0.80           29.808         29.805         25.735           9.322         9.321         7.921           397.18         397.15         398.94           0.1597         0.1595         0.2132           0.4764         0.4764         0.4744           0.3168         0.3169         0.2611           313.16         313.15         335.44           0.206         0.206         0.216           3         5         2

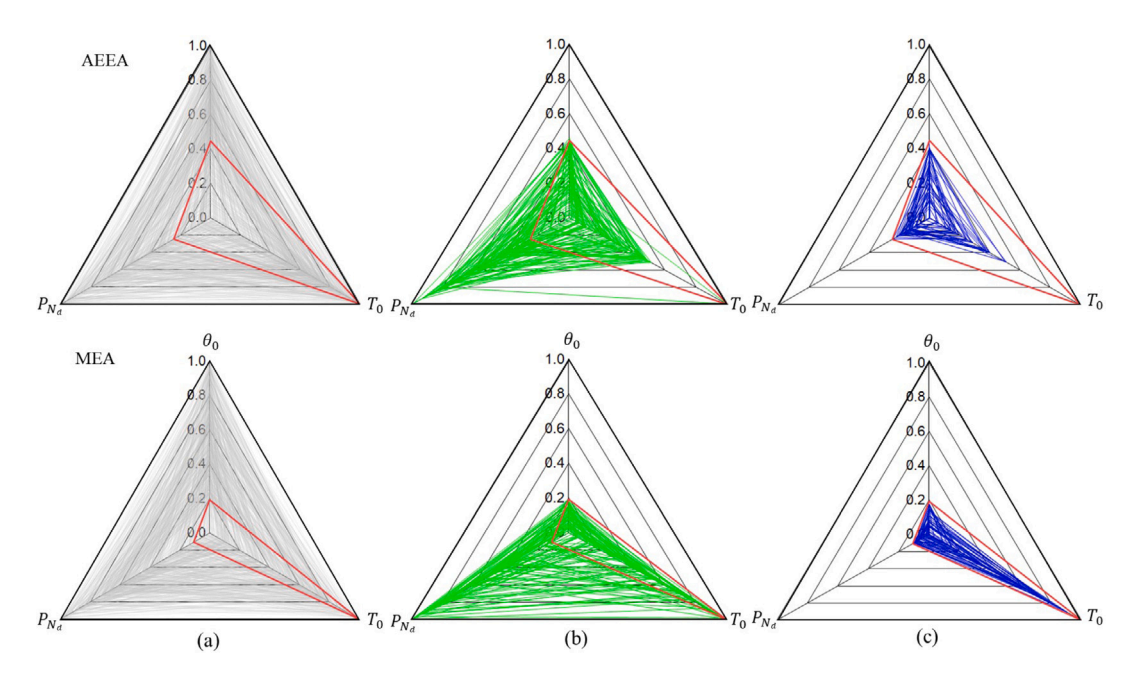


Fig. 8. Spider plots displaying the normalized values of each process variable ( $\theta_0$ ,  $P_{N_d}$ ,  $T_0$ ) for AEEA (top) and MEA (bottom). The largest black triangles represent the initial normalized bounds on  $\theta_0$ ,  $P_{N_d}$ ,  $T_0$ , and solid red triangles represent the tightened bounds obtained by solving the feasibility tests. Process simulations for 500 combinations of the process variables for each solvent are represented on the spider plots, depending on the simulation outcome: (a) simulations that fail to converge (assumed infeasible, gray), (b) operating conditions that violate the design constraints (infeasible, green), and (c) operating conditions that result in a converged simulation (feasible, blue).

Table 7
Molecular design space defined for each design case. DS denotes a design case.

Parameter	$n_t^U$	$n_{G_A}^L$	$n_{G_A}^U$	$n_{\mathrm{OH}}^U$	$n_{\mathrm{iso}}^U$	$N_{\rm max,slack}$	$N_{\rm max, unq}$
DS1	12	1	1	3	2	5	50
DS2	12	1	2	3	4	8	100
DS3	12	1	3	3	4	8	100

initial lean-solvent loading is 0.3995 for both S4 and S5. While the original lean-solvent loading of 0.4 used in run S4 is only slightly outside the feasible region, the solver fails to find a feasible point nonetheless. The effectiveness of the feasibility tests is also highlighted in the case of AMPD. As reported in Table 6, equivalent solutions are obtained using the algorithm with and without feasibility tests for AMPD after the 5 runs. We observe that the optimizations without the tests encounter numerical failures either during the course of the algorithm (S1) or at the start of the algorithm (S4 and S5). On the

**Table 8**Computational performance of the algorithm with feasibility tests for three design cases, averaged over 50 runs for each design case. The calculation of percentage of molecules failing in each test is based on the total number of molecules explored during the optimization runs.

	DS1	DS2	DS3
Average number of iterations	16.67	20.90	20.10
Average number of molecules failing a test	2.56	1.50	0.30
Percentage of molecules failing in Test 1 (%)	12.63	2.42	0.20
Percentage of molecules failing in Test 2 (%)	9.47	9.68	0.00
Percentage of molecules failing in Test 3 (%)	0.00	0.00	0.00
Percentage of molecules failing in Test 4 (%)	2.11	0.00	0.10
Average CPU time (s)	3186.6	6628.9	5846.3

other hand, successful convergence to a solution of the primal problem for AMPD is obtained with the introduction of feasibility tests for all five user-provided starting points. The average computational time is slightly decreased (by 10%), potentially as a consequence of the

Table 9

The top five candidate molecular structures for DS1 identified by minimizing the total annualized cost using the proposed CAMPD approach with integer cuts. The structural features of the candidate solvents are provided in Fig. A.13. The total annualized cost (TAC), total cost of investment (TCI) and operating cost (OPEX) are in units of US million dollars per year (\$million year<sup>-1</sup>). The total energy consumption of the process ( $Q_{total}$ ) is presented in units of GJ ton-CO $_2^{-1}$ . MEA is in the last row as a benchmark solvent.

Rank	Solvent name or molecular code (short code)	TAC	TCI	OPEX	$Q_{ m total}$
1	2-(2-hydroxyethylamino)ethanol (DEA)	17.577	5.818	11.144	4.969
2	2-aminopropane-1,3-diol (2APD)	23.108	7.735	14.758	7.261
3	3-(3-hydroxypropylamino)propan-1-ol (3HPAP)	24.799	9.000	15.183	8.160
4	2-(aminomethyl)propane-1,3-diol (2AMPD)	24.996	8.541	15.840	7.800
5	2-amino-2-methyl-1,3-propanediol (AMPD)	25.735	8.952	16.167	7.926
Ref.	2-aminoethanol (MEA)	29.806	8.047	21.144	9.323

**Table 10**Detailed results of the top five solutions of the integrated solvent and chemical absorption process design for DS1. The molecules are presented in the order of high to low rank with their short name. MEA is in the first column as a benchmark solvent.

	DS1					
Optimal Value	MEA (ref.)	DEA	2APD	ЗНРАР	2AMPD	AMPD
TAC (\$million year <sup>-1</sup> )	29.806	17.577	23.108	24.799	24.996	25.735
CAPEX (\$million year <sup>-1</sup> )	8.048	5.818	7.735	9.000	8.541	8.952
OPEX (\$million year <sup>-1</sup> )	21.144	11.144	14.758	15.183	15.840	16.167
$Q_{\text{total}}$ (GJ ton-CO <sub>2</sub> <sup>-1</sup> )	9.323	4.969	7.261	8.160	7.800	7.926
Sol circ. rate (kg h <sup>-1</sup> )	0.3731	0.2992	0.4308	0.4816	0.4658	0.4637
Reboiler temperature (K)	397.18	386.95	398.94	385.87	398.81	398.98
Cyclic capacity (mol mol-1)	0.160	0.321	0.200	0.254	0.212	0.213
Rich loading (mol mol-1)	0.476	0.341	0.471	0.345	0.475	0.474
Lean loading, $\theta_0$ (mol mol <sup>-1</sup> )	0.317	0.020	0.271	0.090	0.262	0.261
Lean temperature, $T_0$ (K)	313.15	334.54	335.51	316.86	335.07	335.43
$P_{N_d}$ (MPa)	0.206	0.153	0.213	0.166	0.218	0.216
$Q_{\text{reh}}$ (MW)	209.33	168.35	217.53	194.08	231.46	234.19
$Q_{\rm cond}$ (MW)	-99.585	-49.603	-101.001	-52.745	-110.698	-113.509
Solvent loss (kg ton-CO <sub>2</sub> <sup>-1</sup> )	3.10	$6.92 \times 10^{-2}$	$3.58\times10^{-3}$	$2.37\times 10^{-2}$	$4.00 \times 10^{-3}$	$6.78 \times 10^{-3}$

reduction in the ranges of the design variables achieved in Tests 3 and 4.

These results demonstrate the importance of identifying feasible process conditions for a given solvent to avoid algorithmic failure. In the context of solving MINLP CAMPD problems, one possible approach to resolve numerical failures that occur during the evaluation of process performance in the absence of the tests is to add an integer cut to the master problem in order to eliminate the solvent in question, so that the algorithm focuses the search on other solvent candidates. However, this is not only computationally expensive, but it may also lead to the unnecessary elimination of a promising solvent candidate (note the TAC for AMPD is lower than that of MEA). Furthermore, the introduction of an integer cut does not guarantee that a feasible solvent/process combination can be identified in a subsequent iteration. The robustness achieved through the introduction of the feasibility tests is likely to be critically important in molecular and process design problems where many candidates solvents are infeasible or where the evaluation of the primal problems is computationally expensive.

# 5.2. Overall performance: Application to CAMPD problems

The proposed algorithm is applied to three design cases to identify the best-performing solvents. Each design case (DS) is different in that the maximum allowed number of amine groups is specified as  $n_{G_A}^U=1$ , 2 or 3 in an attempt to consider different amine functionalities in the solvent molecule. Information on the molecular design space, process parameters, bounds on process variables, and algorithmic parameters are given in Tables 3 and 7.

Given the nonconvex nature of the problem, the CAMPD algorithm is run from ten starting points for each design case to explore diverse search directions, thus increasing the likelihood of obtaining globally optimal solvents for each DS. The starting points are chosen from the studies of Bernhardsen and Knuutila (2017) and Papadopoulos et al.

(2016) which yield chemically feasible molecular structures and are known to yield feasible process designs for the process configuration considered, albeit using different process models. The list of starting points is given in Table A.16 in Appendix A.2. Following the termination of the algorithm from all starting points, the solvent that presents the lowest TAC value is reported as an optimal solution. Although multiple initial guesses are used, this does not guarantee the global optimality of the solution. Furthermore, the solution generated is specific to the process specifications and modeling assumptions, and thus it is desirable to generate a list of candidate solvents from which highperforming solvents can be selected for further evaluation by means of other simulation settings (e.g., more detailed models) or experiments. Once the best-known solvent is obtained by solving the MINLP from ten starting points, the solvent structure is added to an integer cut in the master problem and then the algorithm is restarted to generate the next-best solvent from the multiple starting points.

The computational performance of the proposed algorithm is summarized in Table 8 and the detailed results are reported in Tables 9-14. Throughout the discussion, performance metrics for each DS are calculated as an average over 50 simulations corresponding to the generation of five top-ranked solvents from the ten starting points (molecules). All 150 runs carried out converge successfully to locally optimal solutions regardless of the starting point used. From Table 8, it can be seen that different tests are active in each DS. The introduction of feasibility tests successfully eliminates infeasible molecules and process conditions from the design space, making it possible to evaluate feasible molecules in the primal problem without encountering numerical difficulties. The infeasibilities are more prominent for DS1 and DS2, as some of molecules such as alkylamines are found to undergo an undesirable liquid-liquid phase split at the absorber operating conditions. These are successfully avoided in DS3 as the master problem generates a larger proportion of feasible candidates.

Table 11

The top five candidate molecular structures for DS2 identified by minimizing the total annualized cost using the proposed CAMPD approach with integer cuts. The structural features of the candidate solvents are provided in Fig. A.13. The total annualized cost (TAC), total cost of investment (TCI) and operating cost (OPEX) are in units of US million dollars per year (\$million year<sup>-1</sup>). The total energy consumption of the process ( $Q_{\text{total}}$ ) is presented in units of GJ ton-CO<sub>2</sub><sup>-1</sup>. MEA is in the last row as a benchmark solvent. Solutions 1 and 4 are not given specific chemical names as several isomers can be formed from the groups selected.

Rank	Solvent name or molecular code (short code)	TAC	TCI	OPEX	$Q_{ m total}$
1	$[NH_2C=1,NHCH_2=1,CH_3=2,OH=1]$ (SOL1)	17.144	5.327	11.202	4.785
2	2-(2-hydroxyethylamino)ethanol (DEA)	17.577	5.818	11.144	4.969
3	2-(2-aminoethylamino)ethanol (AEEA)	17.991	5.544	11.832	5.356
4	$[NH_2CH_2=2,C=1,OH=2]$ (SOL2)	19.599	6.186	12.799	6.390
5	1,3-diamino-2-propanol (DAP)	19.754	6.091	13.048	6.645
Ref.	2-aminoethanol (MEA)	29.806	8.047	21.144	9.323

Table 12
Detailed results for the top five solutions of the integrated solvent and chemical absorption process design for DS2. The molecules are presented in the order of high to low rank with their short name. MEA is in the first column as a benchmark solvent.

Optimal value	DS2					
	MEA (ref.)	SOL1	DEA	AEEA	SOL2	DAP
TAC (\$million year <sup>-1</sup> )	29.806	17.144	17.577	17.991	19.599	19.754
CAPEX (\$million year <sup>-1</sup> )	8.048	5.327	5.818	5.544	6.186	6.091
OPEX (\$million year <sup>-1</sup> )	21.144	11.202	11.144	11.832	12.799	13.048
$Q_{\text{total}}$ (GJ ton-CO <sub>2</sub> <sup>-1</sup> )	9.323	4.785	4.969	5.356	6.390	6.645
Sol circ. rate (kg h <sup>-1</sup> )	0.3731	0.1990	0.2992	0.2272	0.3299	0.3055
Reboiler temperature (K)	397.18	400.99	386.95	402.15	398.69	398.60
Cyclic capacity (mol mol-1)	0.160	0.503	0.321	0.446	0.316	0.294
Rich loading (mol mol-1)	0.476	0.936	0.341	0.979	0.929	0.932
Lean loading, $\theta_0$ (mol mol <sup>-1</sup> )	0.317	0.432	0.020	0.533	0.613	0.638
Lean temperature, $T_0$ (K)	313.15	333.76	334.54	333.67	335.84	335.33
$P_{N_{\star}}$ (MPa)	0.206	0.246	0.153	0.253	0.211	0.216
$Q_{\text{reb}}$ (MW)	209.33	163.52	168.35	180.25	191.30	194.42
Q <sub>cond</sub> (MW)	-99.585	-46.344	-49.603	-54.675	-89.000	-97.081
Solvent loss (kg ton-CO <sub>2</sub> <sup>-1</sup> )	3.10	$3.70 \times 10^{-1}$	$6.92 \times 10^{-2}$	$1.75 \times 10^{-1}$	$7.86 \times 10^{6}$	$1.61 \times 10^{-1}$

It is clear from Table 8 that the computational cost of solving the overall CAMPD is high even for the smaller design space (3186 s for DS1, 6628 s for DS2, and 5846 s and for DS3), suggesting that the computational cost would be significantly increased if many infeasible combinations of molecular structures and process conditions were explored in the absence of feasibility tests. User-provided initial guesses are found to be infeasible for some molecular candidates. For example, the initial value of the lean loading for MDEA is automatically updated by the algorithm to  $0.05 \text{ mol mol}^{-1}$  from  $0.15 \text{ mol mol}^{-1}$ , allowing the process performance to be successfully assessed for this solvent though the solution of the primal problem. Without the feasibility tests, the initialization of the process model may fail and incorrectly result in MDEA being considered an infeasible molecule. The overall statistics indicate that the feasibility tests are particularly important when the process optimization incurs a high computational cost; they make it possible to avoid the unnecessary evaluation of infeasible molecules in the primal problem; the role of the feasibility test in providing a feasible initial combination of process conditions for those molecules that pass the tests is critical to the convergence of the problem. The overall reliability achieved in solving many instances of the entire CAMPD algorithm while exploring a large space of solvent structures and their associated process performance highlights the effectiveness of each step of the algorithm developed in Section 5.1.

# 5.3. Optimal solvents identified using the proposed approach

### 5.3.1. Design case 1

In DS1, DEA is identified as the best solvent with a TAC of 17.577 \$million year<sup>-1</sup>, while other top-ranked solvent candidates, with molecular structures shown in Fig. A.13, exhibit higher TAC values (31%–46% higher than that of DEA in Table 10 and Fig. 9(a)). The heat requirement and the total cost of the process with DEA are decreased by 41% and 47%, respectively, relative to those with MEA. This large reduction in cost is achieved through higher cyclic capacity and lower

reboiler duty in the desorber, leading to a significant decrease in the total energy requirement of the system. It is noteworthy that a high cyclic capacity is obtained with DEA in spite of the low solubility of CO2 in aqueous mixtures of DEA. In Fig. 10, the CO2 partial pressure predicted by the SAFT-y Mie approach used in the current work is shown as a function of CO<sub>2</sub> loading at two different temperatures (313 K and 383 K). At a fixed partial pressure of CO<sub>2</sub>, it can be seen that DEA exhibits very low CO<sub>2</sub> loading at 313 K. However, a high purity of the regenerated solvent, i.e., a low lean loading, is attainable with a low reboiler duty, resulting in a high cyclic capacity (0.321 mol mol<sup>-1</sup> for DEA and 0.160 mol mol<sup>-1</sup> for MEA at the optimal process conditions, see Table 10). As a result, the solvent circulation rate, equipment size, and total energy consumption are decreased. As reported in Ramachandran et al. (2006), the process with MEA is indeed known to use a large amount of energy for solvent regeneration due to the formation of a highly stable carbamate in the absorber. Interestingly, no tertiary amine is identified in the list of optimal solvents, although a low regeneration energy and a high theoretical absorption capacity are expected for these molecules (Chowdhury et al., 2013). This is likely due to the higher molecular weight associated with the bulky alkyl group, CH<sub>3</sub>, attached to the nitrogen atom resulting in a lower molar concentration of the tertiary amine in the mixture under the assumptions made in the problem formulation. The absence of tertiary amines from the list of top five solvent may also be explained by the fact that the absorption capacity of these solvents is greatly influenced by the partial pressure of CO<sub>2</sub>. For example, the CO<sub>2</sub> solubility in aqueous MDEA at low partial pressures (P 

10 kPa) is similar or significantly less than that in MEA and DEA. It is worth mentioning that the highest achievable CO<sub>2</sub> partial pressure in the absorber for the given process specifications is approximately 5 kPa, which is estimated by multiplying the absorber operating pressure and the mole fraction in CO<sub>2</sub> of the flue gas stream. Similar discussions can be found in the study of Bernhardsen and Knuutila (2017) in which absorption capacity, cyclic capacity and basicity (pKa) of 132 aqueous amine solvents available in the literature

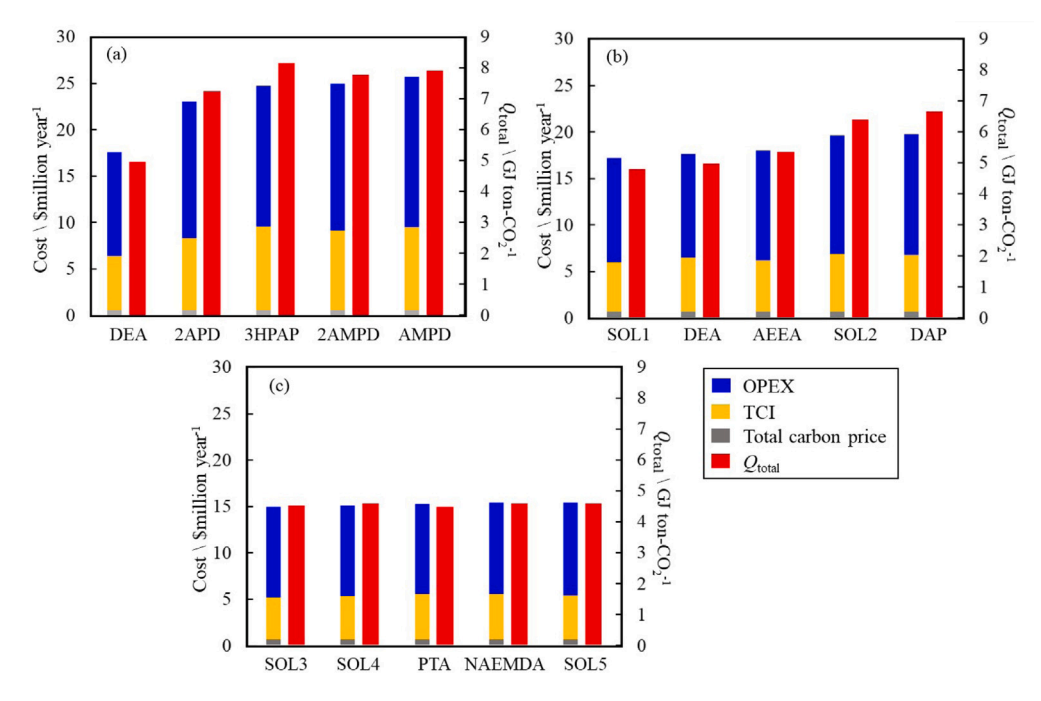


Fig. 9. Comparison of the overall process performance of the top five solvents identified using the proposed CAMPD approach for (a) DS1, (b) DS2, and (c) DS3. For each solvent, the bar on the left denotes the TAC, broken down into OPEX (blue), TCI (yellow) and total carbon price (gray), and the bar on the right denotes the total energy requirement ( $Q_{\text{total}}$ ). The cost scale is shown on the left of each plot and the energy scale on the right.

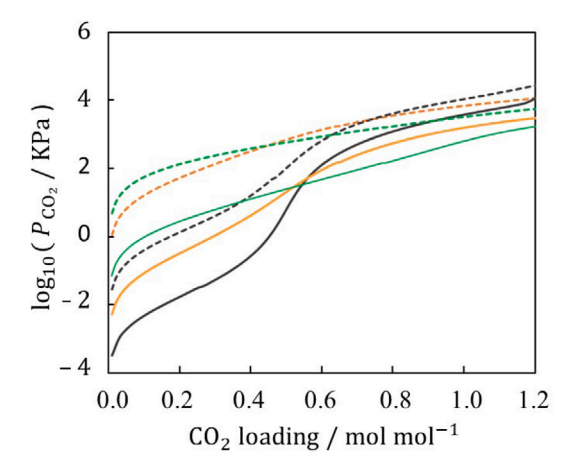


Fig. 10. Partial pressure of  $CO_2$  as a function of  $CO_2$  loading for a 30 wt% (mass) aqueous solution of MEA (dark gray), DEA (yellow) and MDEA (green) as calculated with the SAFT- $\gamma$  Mie EOS. The solid and dashed curves correspond to temperatures of 313 K and 383 K, respectively.

were compared. The authors reported that the cyclic capacity of the best primary and secondary amines is higher than that of any tertiary amine.

### 5.3.2. Design case 2

In DS2, solvent molecules can contain up to two amine groups, so that the design space of DS1 is a subset of that for DS2. With the exception of DEA, all highly-ranked solvents are diamines (see Table 12, Figs. 9(b) and A.13), which comprise two amino groups that participate in the  $\rm CO_2$  removal reactions and thus enable higher  $\rm CO_2$  loadings to be achieved. According to the work of Choi et al. (2014), where the performance of aqueous blends of MDEA and multiamine (alkyl-) solvents with primary and secondary amino groups was investigated, the stability of the carbamate ions decreases in the following

order: primary carbamate > primary–primary dicarbamate > primary–secondary dicarbamate. This implies that the energy required to break the bonds of a dicarbamate is lower than that required for a carbamate. This is one possible explanation as to why a lower heat of regeneration is observed with diamine solvents. The higher cyclic capacity at the optimal process conditions shown in Table 12 corresponds to a lower solvent circulation rate, allowing one to reduce the equipment and operating costs.

The molecular weights of all high-performing solvents are within a range of 104-118 g mol<sup>-1</sup>, i.e., the molecular size is kept as small as possible, while including two amino groups. This trend may be due to the use of a fixed weight concentration of solvent in the problem formulation and to the large impact of the circulation rate on both the cost and energy consumption. As a result, the algorithm towards smaller molecular structures in order to decrease the amount of solvent, while maximizing the number of amino groups. The use of large molecules can lead to an increase in the reboiler operating temperature and is also characterized by a larger solvent viscosity, resulting in relatively large process units and a greater risk of thermal degradation, although this latter aspect is not included in the formulation. It is also noticeable that no alkylamine is included in the list in Table 11. Many of the alkylamines are found to be immiscible with water at the absorber operating conditions (see Table 4) and hence they are removed from consideration in the feasibility tests. Although not shown here, the feasible dialkylamines that are explored in the course of the algorithm lead to a slightly higher TAC at the optimal solution of the problem, whilst their cyclic capacity and energy consumption are similar to or less than those of some of the highly-ranked solvents. The increase in TAC with alkylamines is caused by the larger amine losses to the atmosphere at the top of the absorber and desorber, which increase the operating costs for amine make-up. For example, the TCI and total energy consumption for 1,3-propanediamine (CAS registry number: 109-76-2), one of the solvents evaluated during the search, are lower than those of its hydroxyl-containing analog, 1,3-diamino-2-propanol (CAS registry number: 616-29-5), by 4.9 and 7.0%, respectively. However, the cost for amine make-up is greater by 98.7%, which outweighs the smaller TCI and energy consumption. This is because the addition

Table 13

The top five candidate molecular structures for DS3 identified by minimizing the total annualized cost using the proposed CAMPD approach with integer cuts. The structural features of the candidate solvents are provided in Fig. A.13. The total annualized cost (TAC), total cost of investment (TCI) and operating cost (OPEX) are in units of US million dollars per year (\$million year<sup>-1</sup>). The total energy consumption of the process ( $Q_{total}$ ) is presented in units of GJ ton- $CO_2^{-1}$ . MEA is in the last row as a benchmark solvent. Solutions 1, 2 and 5 are not given specific chemical names as several isomers can be formed from the groups selected.

Rank	Solvent name or molecular code (short name)	TAC	TCI	OPEX	$Q_{ m total}$
1	$[NH_2CH_2=2,NHCH=1,CH=1,OH=2]$ (SOL3)	14.872	4.509	9.748	4.492
2	[NH2CH2=2,NHCH=1,OH=1] (SOL4)	15.041	4.597	9.829	4.571
3	propane-1,2,3-triamine (PTA)	15.148	4.875	9.658	4.458
4	N'-(aminomethyl)-N'-methylmethanediamine (NAMDA)	15.278	4.859	9.804	4.569
5	$[NH_2CH_2=2,NHCH_2=1,C=1,OH=2]$ (SOL5)	15.288	4.720	9.953	4.577
Ref.	2-aminoethanol (MEA)	29.806	8.047	21.144	9.323

**Table 14**Detailed results for the top five solutions of the integrated solvent and chemical absorption process design for DS3. The molecules are presented in the order of high to low rank with their short name. MEA is in the first column as a benchmark solvent.

Optimal value	DS3					
	MEA (ref.)	SOL3	SOL4	PTA	NAEMDA	SOL5
TAC (\$million year <sup>-1</sup> )	29.806	14.872	15.041	15.148	15.278	15.288
CAPEX (\$million year <sup>-1</sup> )	8.048	4.509	4.597	4.875	4.859	4.720
OPEX (\$million year <sup>-1</sup> )	21.144	9.748	9.829	9.658	9.804	9.953
$Q_{\text{total}}$ (GJ ton-CO <sub>2</sub> <sup>-1</sup> )	9.323	4.492	4.571	4.458	4.569	4.577
Sol circ. rate (kg h <sup>-1</sup> )	0.3731	0.1902	0.1759	0.1698	0.1547	0.1937
Reboiler temperature (K)	397.18	401.12	401.64	401.81	401.28	401.12
Cyclic capacity (mol mol-1)	0.160	0.692	0.600	0.538	0.571	0.681
Rich loading (mol mol <sup>-1</sup> )	0.476	1.394	1.410	1.378	1.154	1.402
Lean loading, $\theta_0$ (mol mol <sup>-1</sup> )	0.317	0.702	0.810	0.839	0.583	0.721
Lean temperature, $T_0$ (K)	313.15	334.98	335.12	338.66	337.95	334.85
$P_{N_{\star}}$ (MPa)	0.206	0.235	0.241	0.221	0.215	0.236
$Q_{\text{reb}}$ (MW)	209.33	152.38	152.16	145.07	146.62	154.62
$Q_{\rm cond}$ (MW)	-99.585	-44.668	-48.330	-50.455	-53.808	-46.154
Solvent loss (kg ton-CO <sub>2</sub> <sup>-1</sup> )	3.10	$2.32\times10^{-7}$	$6.31 \times 10^{-4}$	$3.67\times 10^{-3}$	$2.52\times10^{-2}$	$2.74\times10^{-7}$

of hydroxyl groups in the amine facilitates the formation of hydrogen bonds with water, making the amine more soluble in water and less volatile. Care must be taken, however, when considering the introduction of hydroxyl groups in the molecular structure, as the increase in the number of hydroxyl groups has an adverse effect on the heat duty for regeneration and  $CO_2$  solubility, as demonstrated in the experimental study of Muchan et al. (2017).

### 5.3.3. Design case 3

In DS3, the larger molecular design space of molecules with up to three amine groups is explored. As can be seen in Tables 13 and 14, and in Fig. 9, only triamines that have multiple reaction sites and form various species of carbamate or bicarbonate with CO2 appear in the list of high-performance solvents. Molecules with a higher number of amine groups lead to a high CO2 loading in the rich solvent and a low regeneration energy, resulting in lower steam costs for regeneration, which constitute a major component of the TAC with a share of 40%-45%. A significant reduction in the TAC of the top-ranked solvents is achieved due to the increased cyclic capacity. The TAC with SOL3 is decreased by 50.1% compared to MEA, and 13.2% compared to the top ranked solvent (SOL1) in DS2. The cyclic capacity of SOL3 at the optimal process operating conditions is increased by 333.7% compared to MEA, and 37.5% compared to SOL1. As discussed for DS2, the formation of dicarbamates entails a lower heat of reaction than that of the carbamate formed from MEA. In addition, the combined effect of the higher prevalence of weak binding between CO2 and amino groups and the high cyclic capacity results in a relatively low regeneration energy. It can be observed that the solvent structures in the list comprise primary and secondary amines, which may be explained by the fact that the effect of cyclic capacity on the cost dominates compared to the low heat of regeneration that can be derived from the introduction of a tertiary amine group in the molecule.

### 5.4. Comparison between CAMPD and CAMD formulations

Having developed a robust CAMPD algorithm, we now discuss the value of evaluating the molecular properties within the process context. In Fig. 11, we compare the key molecular properties of the top-ranked optimal solvents identified from each DS, in addition to MEA. The properties are selected based on the studies of Papadopoulos et al. (2016) and Lee et al. (2020), where the CAMD problem was formulated as a multi-objective optimization (MOO) problem to identify the tradeoffs (a set of Pareto-optimal solvents) between the desired properties. It is generally assumed that better solvents have a lower saturated vapor pressure  $(P_{vap})$ , a higher liquid density  $(\rho)$ , a lower heat capacity  $(C_p)$ , and a lower relative energy difference (RED). Here, each property is normalized based on its minimum and maximum values so that all values lie in the range 0 to 1. The liquid density is scaled based on  $-\rho$ so that smaller values of all the scaled properties are indicative of better performing solvents. Additionally, the heat of absorption  $(-\Delta H_{abs})$ , which is an indicator of the heat requirement for regeneration, and the CO2 loading, which is an important parameter associated with the absorption capacity of the solvents, are presented for the optimal solvents identified. The heat of absorption is calculated based on the simulation approach proposed by Graham (2020) who aimed to mimic the experimental setting of Arcis et al. (2012), rather than applying the Gibbs-Helmholtz equation. As can be seen in Fig. 11, it is not possible to correlate the performance of the solvents in terms of property targets with the overall performance of processes using these solvents. SOL3, identified as the most cost-effective solvent in the solution of the CAMPD problem, appears as the best solvent only with respect to density and CO2 loading. SOL3 is also the third best molecule in terms of energy efficiency when assessed through the heat of absorption within the range of 0–1 mol mol<sup>-1</sup> of CO<sub>2</sub> loading. However, the results of the CAMPD formulation uncover that SOL3 leads to the most-energy efficient process (lowest value of  $Q_{\rm total}$ ).

Another aspect of interest in the design of the solvent is the vapor pressure of the solvent,  $P_{vap}$ , at 323 K which can be used as an indicator of solvent losses and which should be as low as possible to minimize the environmental impact. Clearly, SOL1 exhibits the lowest vapor pressure in Fig. 11(a). However, the solvent losses calculated as the sum of the amount of the solvent in kg ton- $CO_2^{-1}$  in the clean gas and in the  $CO_2$ gas stream at the optimal process conditions, suggest that SOL3 leads to the lowest value (3.10 for MEA,  $6.92 \times 10^{-2}$  for DEA,  $3.70 \times 10^{-1}$  for SOL1 and  $2.32 \times 10^{-7}$  for SOL3 in units of kg ton-CO<sub>2</sub><sup>-1</sup> captured). The discrepancies in the CAMD and CAMPD approaches demonstrate that the best overall performance of the processing materials can only be realized when the molecular properties are evaluated within integrated molecular-process models. As has been shown, the proposed CAMPD algorithm provides a systematic way of identifying promising solvents in a process that is economically and environmentally favorable, allowing one to quantify the performance of the solvent in the process domain and to embed the trade-offs between properties directly in the decision-making.

# 5.5. Comparison between direct and decomposition-based solution approaches

An important aspect of the proposed CAMPD algorithm is that it considers the process and molecular-level decisions simultaneously. As discussed in the Introduction, alternatives to the direct solution approach that can avoid the numerical difficulties of solving a large MINLP process-molecular model include decomposition-based approaches, also known as two-stage approaches, in which a set of feasible molecular candidates is generated first and subsequently, the most promising candidate molecules are further investigated using a detailed process model. In order to compare the performance of the two-stage approach and the integrated CAMPD approach, we consider the list of potential solvents candidates from the study of Lee et al. (2020) in which 40 Pareto-optimal solvents were generated by solving the multi-objective CAMD problem using the sandwich algorithm (Rennen et al., 2011). The total CPU time taken to generate the set of 40 optimal amine solvents and the average CPU time taken to generate one optimal solution were reported as 353 s and 8.38 s, respectively, in Table 12 of Lee et al. (2020). Among the 40 optimal solvents, the 19 solvents that satisfy the molecular structure constraints for DS3 are further evaluated in the primal problem, i.e., process optimization. The set of structurally feasible molecules and the results of the application of the feasibility tests to these molecules are given in Table A.17 of Appendix A.2. Among the 19 solvents that are structurally feasible, many of the solvents are found to be infeasible for the given process specifications, mainly due to high melting points, high flash points, and immiscibility with water, leaving only seven solvents feasible in the tests.

The overall results of evaluating the process performance of the solvents generated using the decomposition method (design molecules by CAMD, then optimize process performance) and the proposed CAMPD method (design molecules and process simultaneously) are summarized in Fig. 12. As can be seen, the optimal CAMPD solvents in DS1, DS2, and DS3 have better economic performance and energy efficiency on average, exhibiting lower values in all evaluation metrics. Specifically, the average values of TAC and  $Q_{\mathrm{total}}$  are decreased by 39.9% and 28.9%, respectively, when using the CAMPD approach, indicating that the two-stage approach may result in suboptimal solutions in the absence of the systematic strategy of coupling the molecular design and process evaluation. The best solvent among the evaluated solvent candidates is identified as M26, with a corresponding TAC of 16.0 \$million year<sup>-1</sup> (See Table 15), i.e., nearly 8% higher than SOL3. In fact, the optimal TAC value with M26 is higher than that of the top five solvents from DS3 despite the larger molecular design space used in Lee

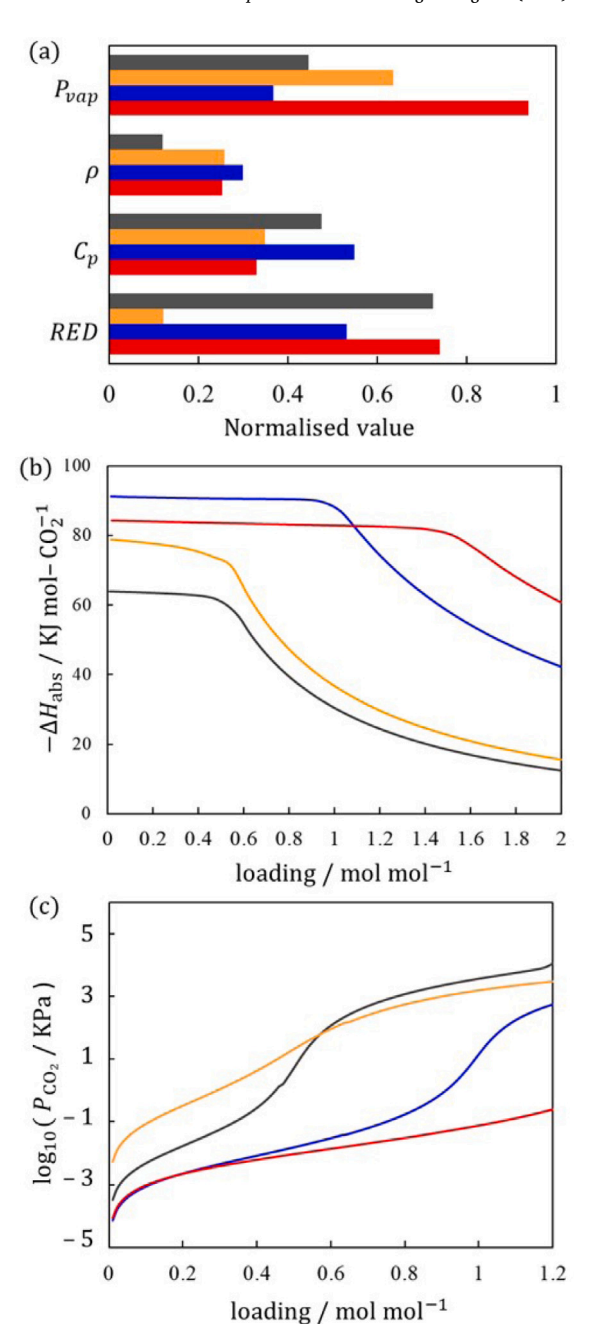


**Fig. 11.** A comparison of the molecular properties of DEA (amber), SOL1 (blue) and SOL3 (red) which are identified as the top solvents in each design case. The properties of MEA (dark gray) are provided as a reference. In (a), normalized value of properties,  $P_{cup}$ ,  $\rho$ ,  $C_p$  and RED are shown. (b) the heat of absorption ( $-\Delta H_{abs}$ ) at 323 K, as a function of CO<sub>2</sub> loading and (c) partial pressure of CO<sub>2</sub> ( $P_{CO_2}$ ) at 313 K, as a function of CO<sub>2</sub> loading predicted using the SAFT- $\gamma$  Mie EOS for 30 wt% (mass) of amine in the aqueous mixture.

et al. (2020). This suggests that the use of the decomposition-based approach can lead to sub-optimal solutions by guiding the exploration of the design space towards limited or biased molecular domains. Nevertheless the TAC value for M26 is larger than any of the DS1 and DS2 solutions, indicating that the CAMD methodology identifies solvents with reasonable performance. Decomposition may also give rise to a high computational cost, as a large number of molecules needs to be enumerated to identify optimal or near optimal solutions. The CPU time taken to evaluate the feasibility tests and primal problem for the 19 solvents is 3422 s, which is less than that of DS3. However, this

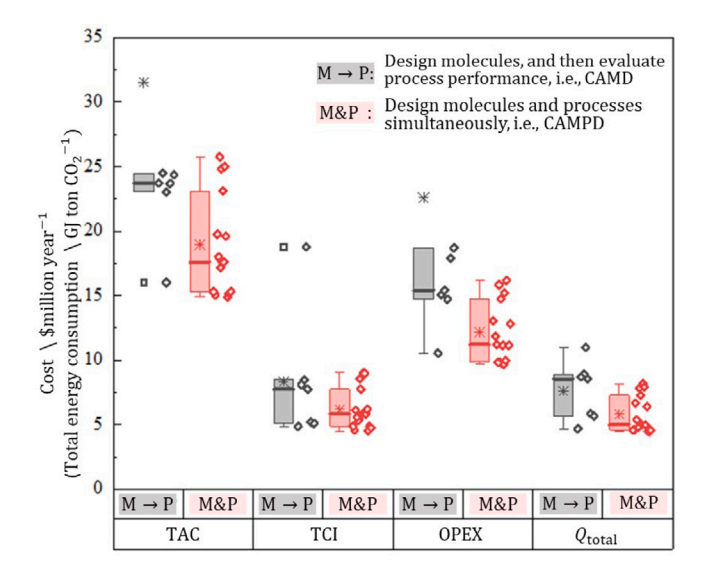


Fig. 12. A comparison of the overall process performance for the optimal solvents generated (i) by solving a MOO CAMD problem and then optimizing the process  $(M \rightarrow P)$  and (ii) by solving the integrated CAMPD problem (M&P). Each box plot is used to display the maximum and minimum values, the first and third quartile ranges, and the median values of the process performance indicators. The values for all solvents used to construct each box plot are shown on the right of the box plot  $(\circ)$  with the mean value indicated by  $\star$ . The TAC and OPEX values (85.3 and 65.9 \$million year $^{-1}$ ) for solvent M32 are omitted from the plot due to their large magnitude.

Table 15 Performance of the  ${\rm CO_2}$  capture process using solvent M26 identified by enumerating the list of 19 molecules generated by solving a MOO CAMD problem (Lee et al., 2020) and evaluating the process performance of those that satisfy the molecular feasibility constraints in problem (1). The molecular code M26 denotes [NHCH=1, NCH<sub>3</sub>=1, NCH<sub>3</sub>=1, CH<sub>4</sub>=3, OH=1].

Parameters	Value
Optimal solvent	M26
TAC (\$million year <sup>-1</sup> )	16.007
TCI (\$million year <sup>-1</sup> )	4.851
OPEX (\$million year <sup>-1</sup> )	10.541
$Q_{\text{total}}$ (GJ ton-CO <sub>2</sub> <sup>-1</sup> )	4.676
Solvent circ. rate (kg h <sup>-1</sup> )	0.166
Cyclic capacity (mol mol <sup>-1</sup> )	0.806
Lean loading, $\theta_0$ (mol mol <sup>-1</sup> )	0.204
Lean solvent temperature, $T_0$ (K)	333.59
Desorber pressure, $P_{N_{\star}}$ (MPa)	0.234
Total CPU time (s)	3422

saving results in part from the presence of infeasible molecules that fail to pass the feasibility tests in the course of the algorithm. It also does not account for the cost of generating the set of Pareto-optimal solvents. In summary, there is clear evidence that the proposed CAMPD algorithm offers a more reliable way to identify promising solvents with the desired overall performance.

# 6. Conclusions

In our current work, a robust CAMPD framework has been proposed for the simultaneous design of optimal aqueous solvents and  $\mathrm{CO}_2$  chemical absorption–desorption processes. The focus of the development has been to overcome the numerical challenges that arise due to the complex nonlinear interactions between process models and molecular structure–property models. This is particularly relevant in chemical absorption as the highly non-ideal behavior of the solvent–water– $\mathrm{CO}_2$  mixtures, including chemical reactions and the potential to exhibit LLE/VLLE, requires the use of advanced predictive thermodynamic models, such as the SAFT- $\gamma$  Mie approach used here. New feasibility tests have been combined with the primal problem of the OA algorithm to provide a reliable way to assess the best process performance for a

given solvent by removing infeasible process conditions and molecular structures from the search space before attempting to solve the process optimization problem. Through the application of the feasibility tests over a set of more than 4000 molecules, the tests have been found to be robust and to lead to the elimination of infeasible process conditions. Perhaps more importantly, the tests also generate new (tighter) bounds on the process variables and starting points. These values are tailored to each candidate solvent to ensure process feasibility and their use has been shown to increase the reliability of the process optimizations significantly, regardless of the user-provided starting point.

The efficiency and robustness of the proposed CAMPD algorithm has been demonstrated by studying the design of a  $\rm CO_2$  chemical absorption process for a 400 MWe combined CCGT power plant (Bailey and Feron, 2005) where the solvent molecular structure and the process operating conditions have been simultaneously optimized to maximize the overall economic performance of the process. A systematic investigation of the performance of the proposed CAMPD algorithm over 150 runs has shown that the feasibility tests enhance robustness and increase the likelihood of identifying high-performance solutions. By identifying infeasible regions within molecular and process domains, numerical errors are prevented over the course of the exploration, which leads to a reduction in the computational cost of solving the full CAMPD MINLP.

Three design spaces were considered in the course of the study, covering different subsets of the space of amines. For each design space, the top five candidate solvents were generated and their detailed performance was discussed in the context of previous studies. The results have highlighted the importance of a high cyclic capacity, a quantity which depends both on the nature of the solvent and on the process operating conditions, reinforcing the importance of the interactions between the molecular and process scales. Performance metrics that relate both to economics and environmental impact, such as energy consumption or solvent losses per ton of  $\mathrm{CO}_2$  capture, were found to show favorable behavior for the optimal solvents identified.

Furthermore, we have investigated the value of solving the CAMPD MINLP as an integrated problem in which optimal decisions are made simultaneously. While such an approach may appear burdensome due to the size and nonlinearity of the problem, we have found that key process performance indicators do not correlate well with those solvent properties that are often taken as indicators of a high-performance solvent. We have also compared process performance for optimal solventprocess combinations found via the direct solution of the CAMPD and those found via a decomposition-based approach in which solvents are selected on the basis of property targets and the process is then optimized for these candidates. While good process performance was achieved using the decomposition approach, the simultaneous consideration of molecular and process-level decisions was found to yield better solutions. Even when considering a smaller design space in the simultaneous approach than in the decomposition approach, it was found that reductions in the total annualized cost of 1.2 million USD per year (7%) and in the energy consumption of 4% could be achieved with the integrated approach. It is expected that even greater savings would be achieved by widening the CAMPD design space.

The availability of a robust approach to the simultaneous solution of CAMPD problem opens the way to gain a better understanding of the interactions between molecular and process-level decisions. In particular, it is now possible to investigate the effect of various choices of process specifications, such as high or low concentration of CO<sub>2</sub> in the flue gas, and of process configuration on the optimal designs obtained. Given the predictive capabilities of the SAFT-γ Mie EOS, it would be useful to extend the molecular search domain to a more diverse set of functional groups, for example, ionic liquids, which have been found to offer promise for CO<sub>2</sub> capture (Gurkan et al., 2010; Chong et al., 2017; Silva-Beard et al., 2022), or cyclic amines, which have been widely used as rate-promoting additives and which can also be used as phase-change solvents. The latter will require the introduction of

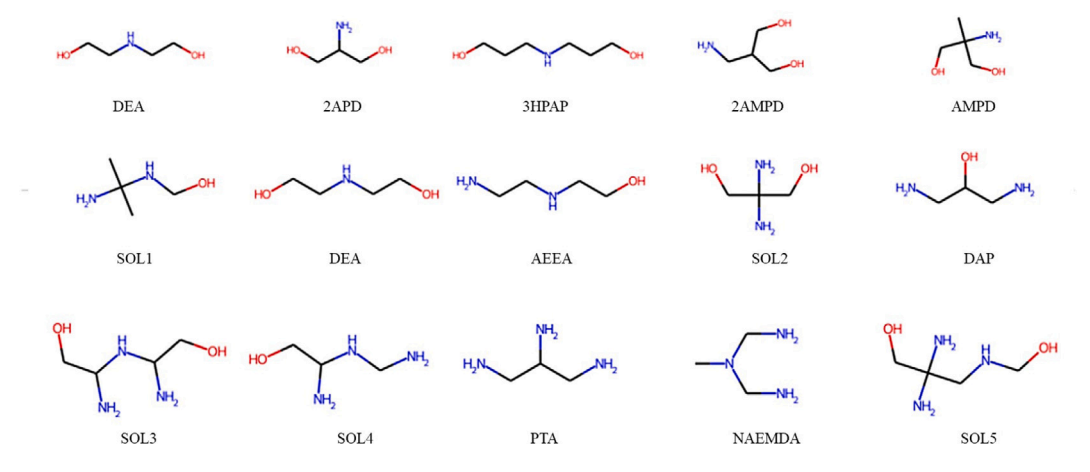


Fig. A.13. Representation of the molecular structures of the top five solvents for DS1, DS2, and DS3. SOL1-SOL5 can form several isomers from the groups selected but only one is shown.

new feasibility tests. It is worth mentioning that the lack of a standard evaluation platform makes the fair comparison of the validity and applicability of CAMPD algorithms challenging. The development of a standard benchmark problem library and associated evaluation metrics would thus be beneficial to gauge the quality of solution approaches proposed in our work and by others. Finally, it would be useful to study the effect of adding other key performance criteria as objective functions in a multi-objective optimization formulation to optimize the solvent structures and process conditions against conflicting objectives that take into account environmental and safety performance as well as economic aspects.

# CRediT authorship contribution statement

Ye Seol Lee: Conceptualization, Methodology, Software, Validation, Investigation, Data curation, Writing – original draft, Visualization. Amparo Galindo: Conceptualization, Methodology, Validation, Writing – review & editing, Supervision. George Jackson: Conceptualization, Methodology, Writing – review & editing, Supervision. Claire S. Adjiman: Conceptualization, Methodology, Validation, Writing – review & editing, Supervision.

# Declaration of competing interest

The authors declare that they have no known competing financial interests or personal relationships that could have appeared to influence the work reported in this paper.

### Data availability

Data will be made available on request.

# Acknowledgments

The authors gratefully acknowledge financial support from Funds For Women Graduates (FfWG) from the British Federation of Women Graduates and the Department of Chemical Engineering at Imperial College London for a Roger Sargent scholarship.

### Appendix A

# A.1. A second-order group interaction in SAFT- $\gamma$ -Mie EOS

As noted in the main text of the article, we define a set of equations to enable the representation of a given a molecule described by a vector n based on the groups in the design space and a vector  $n_S$  using the SAFT- $\gamma$  Mie groups. These equations are listed here for completeness.

The use of second-order groups  $NH_2^*$ ,  $NH^*$  and  $N^*$  is invoked when an alkanolamine is present in the aqueous solution. In addition, the  $CH_2OH_{Short}$  group is introduced when the alkanolamine includes less than three carbons along the carbon backbone, to account for the fact that interactions between the amine and hydroxyl groups, when in close proximity within the solvent molecule, are affected by the presence of water.

To ensure that the second-order interactions of the amine groups and hydroxyl group are accounted for whenever relevant, it is necessary to define a representation of the molecule that is consistent with the SAFT- $\gamma$  Mie definition of groups. It should be noted that when using second-order groups, the like group interactions parameters are unchanged (e.g., NH $_2^*$ -NH $_2^*$  interactions and NH $_2$ -NH $_2$  interactions are identical), and only unlike group interactions parameters are different.

Having introduced the different groups, the translation of amine groups between the two molecular representations, n and  $n_S$ , can be expressed by introducing a binary variable z and imposing the following constraints:

$$\begin{split} \frac{n_{\text{OH}}}{n_{\text{OH}}^U} &\leq z \leq n_{\text{OH}} \\ n_{S,\text{NH}_2} &= (1-z)(n_{\text{NH}_2\text{CH}_2} + n_{\text{NH}_2\text{CH}} + n_{\text{NH}_2\text{C}}) \\ n_{S,\text{NH}} &= (1-z)(n_{\text{NHCH}_3} + n_{\text{NHCH}_2} + n_{\text{NHCH}}) \\ n_{S,\text{N}} &= (1-z)(n_{\text{NCH}_3} + n_{\text{NCH}_2}) \\ n_{S,\text{NH}_2^*} &= z(n_{\text{NH}_2\text{CH}_2} + n_{\text{NH}_2\text{CH}} + n_{\text{NH}_2\text{C}}) \\ n_{S,\text{NH}^*} &= z(n_{\text{NHCH}_3} + n_{\text{NHCH}_2} + n_{\text{NHCH}}) \\ n_{S,\text{N}^*} &= z(n_{\text{NCH}_3} + n_{\text{NCH}_2}) \end{split} \tag{A.1}$$

For the alkyl functional groups, the occurrence of each functional group is identical in both representations, except for the  $CH_2$  group which needs to be adjusted to take into account the  $CH_2OH$  and  $CH_2OH_{Short}$  groups. This can be written as:

$$n_{S,\text{CH}_3} = n_{\text{NHCH}_3} + n_{\text{NCH}_3} + n_{\text{CH}_3}$$
  
 $n_{S,\text{CH}_2} = n_{\text{NH}_2\text{CH}_2} + n_{\text{NHCH}_2} + n_{\text{NCH}_2} + n_{\text{CH}_2} - n_{\text{OH}}$   
 $n_{S,\text{CH}} = n_{\text{NH}_2\text{CH}} + n_{\text{NHCH}} + n_{\text{CH}}$   
 $n_{S,\text{C}} = n_{\text{NH}_3\text{C}} + n_{\text{C}}$ 
(A.2)

The numbers of  $CH_2OH_{Short}$  and  $CH_2OH$  groups are determined by the length of the carbon backbone,  $n_{Carbon}$ , so that when  $n_{Carbon} \leq 2$ , the  $CH_2OH_{Short}$  group is used, and the  $CH_2OH$  group is used otherwise. It is assumed that the longest possible carbon backbone between amine groups and hydroxyl groups governs the proximity effect in aqueous

Table A.16

Molecular starting points given for each case study. The groups are ordered as NH<sub>2</sub>CH<sub>2</sub>, NH<sub>2</sub>CH, NH<sub>2</sub>C, NHCH<sub>3</sub>, NHCH<sub>2</sub>, NHCH<sub>3</sub>, NHCH<sub>3</sub>, NHCH<sub>3</sub>, NHCH<sub>3</sub>, CH<sub>3</sub>, CH<sub></sub>

ID	DS1	DS2	DS3
s1	[1-0-0-0-0-0-0-0-1-0-0-1]	[1-0-0-0-0-0-0-0-1-0-0-1]	[1-0-0-0-0-0-0-0-1-0-0-1]
s2	[0-0-0-0-1-0-0-0-3-0-0-2]	[0-0-0-0-1-0-0-0-3-0-0-2]	[0-0-0-0-1-0-0-0-3-0-0-2]
s3	[0-0-0-0-0-1-0-0-4-0-0-2]	[0-0-0-0-0-0-1-0-0-4-0-0-2]	[0-0-0-0-0-1-0-0-4-0-0-2]
s4	[0-0-0-0-1-0-0-0-5-0-0-2]	[0-1-0-0-0-0-0-0-2-0-0-2]	[1-0-0-0-1-0-0-0-2-0-0-1]
s5	[1-0-0-0-0-0-0-0-3-0-0-1]	[0-0-0-1-0-0-0-0-2-0-0-1]	[1-0-0-0-1-0-0-0-3-0-0-1]
s6	[0-0-0-0-0-0-1-3-3-1-0-1]	[1-0-0-0-1-0-0-0-2-0-0-1]	[0-0-1-0-1-0-0-2-0-0-1]
s7	[0-1-0-0-0-0-0-0-2-0-0-2]	[1-0-0-0-0-0-1-0-5-0-0-2]	[2-0-0-0-1-0-0-0-0-0-1]
s8	[0-1-0-0-0-0-0-1-3-0-0-1]	[0-0-1-0-1-0-0-2-0-0-1]	[0-0-1-1-1-0-0-0-2-1-0-0-0]
s9	[0-0-0-0-0-1-0-1-1-0-0-1]	[0-1-0-0-0-0-0-1-3-0-0-1]	[0-0-1-0-2-0-0-3-2-0-0-0]
s10	[0-0-0-1-0-0-0-0-2-0-0-1]	[0-0-0-0-0-1-0-1-1-0-0-1]	[0-0-1-0-1-0-1-0-3-1-0-0-0]

Table A.17
Results of the feasibility tests when applied to the 19 molecules from CAMD. The molecules are presented in the order of high to low rank with their molecular code. The Test column represents the results of evaluating the molecules in the feasibility tests. The groups are ordered as in Table A.16.

ID	Molecular code	Test
M1	[0-0-0-0-0-0-2-2-0-0-0-2]	Pass
M3	[0-0-0-0-1-0-1-4-0-1-0-1]	Fail
M7	[0-0-0-0-0-0-2-2-2-0-0-2]	Pass
M8	[0-0-0-0-0-0-1-2-0-0-0-1]	Fail
M10	[0-0-0-0-1-0-0-1-2-0-0-0-1]	Pass
M11	[0-0-0-0-2-0-0-1-2-0-0-0-1]	Fail
M12	[0-0-0-0-1-0-1-3-0-0-0-1]	Fail
M16	[0-0-0-0-1-0-0-0-2-4-0-0-0]	Fail
M17	[0-0-0-0-1-0-1-5-1-2-0-1]	Fail
M19	[0-0-0-0-1-0-1-6-3-3-0-1]	Fail
M21	[0-0-0-0-0-0-2-2-1-0-0-2]	Pass
M22	[0-0-0-0-2-0-0-0-1-0-0-0-1]	Pass
M23	[0-0-0-0-2-0-0-0-2-2-0-0-0]	Fail
M25	[0-0-0-0-0-1-0-1-5-0-0-1-1]	Fail
M26	[0-0-0-0-0-1-1-1-3-0-0-0-1]	Pass
M30	[0-0-0-0-0-0-1-3-0-1-0-1]	Fail
M31	[0-0-0-0-1-1-0-0-2-0-0-0-1]	Fail
M32	[0-0-0-0-1-0-0-0-1-0-0-0-1]	Pass
M36	[0-0-0-1-0-1-0-1-3-0-0-0-0]	Fail

solution. The resulting constraints are expressed as:

$$\begin{split} n_{\text{Carbon}} &= n_{S,\text{CH}_2} + n_{S,\text{CH}} + n_{S,\text{C}} \\ 3n_{\text{OH}} - n_{\text{Carbon}} + 1 &\geq \epsilon_n - M_n (1 - y_1) \\ 3n_{\text{OH}} - n_{\text{Carbon}} + 1 &\leq M_n y_1 \\ n_{S,\text{CH}_2\text{OH}} &= (1 - y_1)n_{\text{OH}} \\ n_{S,\text{CH}_2\text{OH}_{\text{Short}}} &= y_1 n_{\text{OH}} \end{split} \tag{A.3}$$

where  $\epsilon_n$  is a small positive number,  $M_n$  is a large positive number and  $y_1$  is a binary variable.

# A.2. Application of the proposed CAMPD algorithm to the ${\rm CO}_2$ chemical absorption process

Table A.16 represents the ten molecules used to initialize the algorithm. Each of the molecules is represented with a molecular code where each number is the occurrence of a functional group.

The molecular structures of the optimal solvents obtained using the proposed CAMPD approach may correspond to several isomers because they are defined by the occurrence of the functional groups in the molecule, without full connectivity information. Therefore, for visualization purposes, some potential molecular structures of the solvents in DS1, DS2, and DS3 are shown in Fig. A.13, without enumerating all possible isomers.

The results of feasibility tests evaluated for the 19 solvents that satisfy the molecular structure constraints of the primal problem for DS3 are summarized in Table A.17. The amine solvents that pass the tests are further evaluated in the process model to assess their overall performance in terms of cost and energy efficiency.

### Appendix B. Supplementary data

Supplementary material related to this article can be found online at https://doi.org/10.1016/j.compchemeng.2023.108204.

### References

Adjiman, C.S., Androulakis, I.P., Floudas, C.A., 2000. Global optimization of mixed-integer nonlinear problems. AIChE J. 46 (9), 1769–1797. http://dx.doi.org/10.1002/aic.690460908.

Adjiman, C.S., Galindo, A., Jackson, G., 2014. Molecules matter: the expanding envelope of process design. In: Computer Aided Chemical Engineering. Vol. 34, Elsevier, pp. 55–64. http://dx.doi.org/10.1016/B978-0-444-63433-7.50007-9.

Adjiman, C.S., Sahinidis, N.V., Vlachos, D.G., Bakshi, B., Maravelias, C.T., Georgakis, C., 2021. Process systems engineering perspective on the design of materials and molecules. Ind. Eng. Chem. Res. 60 (14), 5194–5206. http://dx.doi.org/10.1021/ acs.iecr.0c05399.

Alhajaj, A., Mac Dowell, N., Shah, N., 2016. A techno-economic analysis of post-combustion CO<sub>2</sub> capture and compression applied to a combined cycle gas turbine: Part I. A parametric study of the key technical performance indicators. Int. J. Greenh. Gas Control 44, 26–41. http://dx.doi.org/10.1016/j.ijggc.2015.10.022.

Arcis, H., Ballerat-Busserolles, K., Rodier, L., Coxam, J.-Y., 2012. Measurement and modeling of enthalpy of solution of carbon dioxide in aqueous solutions of diethanolamine at temperatures of (322.5 and 372.9) K and pressures up to 3 MPa. J. Chem. Eng. Data 57 (3), 840–855. http://dx.doi.org/10.1021/je201012e.

Austin, N.D., Sahinidis, N.V., Trahan, D.W., 2016. Computer-aided molecular design:
An introduction and review of tools, applications, and solution techniques. Chem.
Eng. Res. Des. 116, 2–26. http://dx.doi.org/10.1016/j.cherd.2016.10.014.

Bailey, D., Feron, P., 2005. Post-combustion decarbonisation processes. Oil Gas Sci. Technol. 60 (3), 461–474. http://dx.doi.org/10.2516/ogst:2005028.

Bardow, A., Steur, K., Gross, J., 2010. Continuous-molecular targeting for integrated solvent and process design. Ind. Eng. Chem. Res. 49 (6), 2834–2840. http://dx.doi.org/10.1021/ie901281w.

Bernhardsen, I.M., Knuutila, H.K., 2017. A review of potential amine solvents for CO<sub>2</sub> absorption process: Absorption capacity, cyclic capacity and pKa. Int. J. Greenh. Gas Control 61, 27–48. http://dx.doi.org/10.1016/j.ijggc.2017.03.021.

Bommareddy, S., Chemmangattuvalappil, N.G., Solvason, C.C., Eden, M.R., 2010. Simultaneous solution of process and molecular design problems using an algebraic approach. Comput. Chem. Eng. 34 (9), 1481–1486. http://dx.doi.org/10.1016/j. compchemeng.2010.02.015.

Borhani, T.N., Wang, M., 2019. Role of solvents in CO<sub>2</sub> capture processes: The review of selection and design methods. Renew. Sustain. Energy Rev. 114, 109299.

Boston, J., 1980. Inside-out algorithms for multicomponent separation process calculations. In: Computer Applications to Chemical Engineering. In: ACS Symposium Series, Vol. 124, pp. 135–151. http://dx.doi.org/10.1021/bk-1980-0124.ch006.

Bowskill, D.H., Tropp, U.E., Gopinath, S., Jackson, G., Galindo, A., Adjiman, C.S., 2020. Beyond a heuristic analysis: integration of process and working-fluid design for organic Rankine cycles. Mol. Syst. Des. Eng. 5, 493–510. http://dx.doi.org/10. 1039/C9ME00089E.

Burger, J., Papaioannou, V., Gopinath, S., Jackson, G., Galindo, A., Adjiman, C.S., 2015. A hierarchical method to integrated solvent and process design of physical CO<sub>2</sub> absorption using the SAFT-γ Mie approach. AIChE J. 61 (10), 3249–3269. http://dx.doi.org/10.1002/aic.14838.

Buxton, A., Livingston, A.G., Pistikopoulos, E.N., 1999. Optimal design of solvent blends for environmental impact minimization. AIChE J. 45 (4), 817–843. http: //dx.doi.org/10.1002/aic.690450415.

Chao, C., Deng, Y., Dewil, R., Baeyens, J., Fan, X., 2021. Post-combustion carbon capture. Renew. Sustain. Energy Rev. 138, 110490.

Choi, S.Y., Nam, S.C., Yoon, Y.I., Park, K.T., Park, S.-J., 2014. Carbon dioxide absorption into aqueous blends of methyldiethanolamine (MDEA) and alkyl amines containing multiple amino groups. Ind. Eng. Chem. Res. 53 (37), 14451–14461. http://dx.doi. org/10.1021/ie502434m.

- Chong, F.K., Andiappan, V., Ng, D.K.S., Foo, D.C.Y., Eljack, F.T., Atilhan, M., Chemmangattuvalappil, N.G., 2017. Design of ionic liquid as carbon capture solvent for a bioenergy system: Integration of bioenergy and carbon capture systems. ACS Sustain. Chem. Eng. 5 (6), 5241–5252. http://dx.doi.org/10.1021/acssuschemeng.7b00589
- Chowdhury, F.A., Yamada, H., Higashii, T., Goto, K., Onoda, M., 2013. CO<sub>2</sub> capture by tertiary amine absorbents: a performance comparison study. Ind. Eng. Chem. Res. 52 (24), 8323–8331. http://dx.doi.org/10.1021/ie400825u.
- Chremos, A., Forte, E., Papaioannou, V., Galindo, A., Jackson, G., Adjiman, C.S., 2016. Modelling the phase and chemical equilibria of aqueous solutions of alkanolamines and carbon dioxide using the SAFT-γ SW group contribution approach. Fluid Phase Equilib. 407, 280–297. http://dx.doi.org/10.1016/j.fluid.2015.07.052.
- Dufal, S., Papaioannou, V., Sadeqzadeh, M., Pogiatzis, T., Chremos, A., Adjiman, C.S., Jackson, G., Galindo, A., 2014. Prediction of thermodynamic properties and phase behavior of fluids and mixtures with the SAFT-γ mie group-contribution equation of state. J. Chem. Eng. Data 59 (10), 3272–3288. http://dx.doi.org/10.1021/je500248h.
- Duran, M.A., Grossmann, I.E., 1986. An outer-approximation algorithm for a class of mixed-integer nonlinear programs. Math. Program. 36 (3), 307–339. http://dx.doi. org/10.1007/BF02592064.
- Eden, M.R., Jørgensen, S.B., Gani, R., El-Halwagi, M.M., 2004. A novel framework for simultaneous separation process and product design. Chem. Eng. Process.: Process Intensif. 43 (5), 595–608. http://dx.doi.org/10.1016/j.cep.2003.03.002.
- Eljack, F.T., Eden, M.R., Kazantzi, V., Qin, X., El-Halwagi, M.M., 2007. Simultaneous process and molecular design—A property based approach. AIChE J. 53 (5), 1232–1239. http://dx.doi.org/10.1002/aic.11141.
- Fleitmann, L., Kleinekorte, J., Leonhard, K., Bardow, A., 2021. COSMO-susCAMPD: Sustainable solvents from combining computer-aided molecular and process design with predictive life cycle assessment. Chem. Eng. Sci. 245, 116863. http://dx.doi. org/10.1016/j.ces.2021.116863.
- Fletcher, R., Leyffer, S., 1994. Solving mixed integer nonlinear programs by outer approximation. Math. Program. 66 (1), 327–349. http://dx.doi.org/10.1007/ BF01581153.
- Floudas, C.A., 1995. Nonlinear and Mixed-Integer Optimization: Fundamentals and Applications. Oxford University Press.
- Gil-Villegas, A., Galindo, A., Whitehead, P.J., Mills, S.J., Jackson, G., Burgess, A.N., 1997. Statistical associating fluid theory for chain molecules with attractive potentials of variable range. J. Chem. Phys. 106 (10), 4168–4186. http://dx.doi. org/10.1063/1.473101.
- Gopinath, S., 2017. Molecular design, process design and process synthesis of separation systems (Ph.D. thesis). Imperial College London.
- Gopinath, S., Jackson, G., Galindo, A., Adjiman, C.S., 2016. Outer approximation algorithm with physical domain reduction for computer-aided molecular and separation process design. AIChE J. 62 (9), 3484–3504. http://dx.doi.org/10.1002/aic.15411.
- Graham, E.J., 2020. Development of advanced thermodynamic models for  ${\rm CO_2}$  absorption (Ph.D. thesis). Imperial College London.
- Gross, J., Sadowski, G., 2001. Perturbed-chain SAFT: An equation of state based on a perturbation theory for chain molecules. Ind. Eng. Chem. Res. 40 (4), 1244–1260. http://dx.doi.org/10.1021/ie0003887.
- Grossmann, I.E., Viswanathan, J., Vecchietti, A., Raman, R., Kalvelagen, E., et al., 2002. GAMS/DICOPT: a Discrete Continuous Optimization Package. 37, GAMS Corporation Inc, p. 55.
- Gurkan, B., Goodrich, B.F., Mindrup, E.M., Ficke, L.E., Massel, M., Seo, S., Senftle, T.P., Wu, H., Glaser, M.F., Shah, J.K., Maginn, E.J., Brennecke, J.F., Schneider, W.F., 2010. Molecular design of high capacity, low viscosity, chemically tunable ionic liquids for CO<sub>2</sub> capture. J. Phys. Chem. Lett. 1, 3494–3499. http://dx.doi.org/10.1021/jz101533k.
- Gurobi Optimization, LLC, 2022. Gurobi Optimizer Reference Manual. URL https://www.gurobi.com.
- Harper, P.M., Gani, R., Kolar, P., Ishikawa, T., 1999. Computer-aided molecular design with combined molecular modeling and group contribution. Fluid Phase Equilib. 158, 337–347. http://dx.doi.org/10.1016/S0378-3812(99)00089-8.
- Haslam, A.J., González-Pérez, A., Di Lecce, S., Khalit, S.H., Perdomo, F.A., Kournopoulos, S., Kohns, M., Lindeboom, T., Wehbe, M., Febra, S., et al., 2020. Expanding the applications of the SAFT-γ mie group-contribution equation of state: Prediction of thermodynamic properties and phase behavior of mixtures. J. Chem. Eng. Data 65 (12), 5862–5890. http://dx.doi.org/10.1021/acs.jced.0c00746.
- Hostrup, M., Harper, P.M., Gani, R., 1999. Design of environmentally benign processes: integration of solvent design and separation process synthesis. Comput. Chem. Eng. 23 (10), 1395–1414. http://dx.doi.org/10.1016/S0098-1354(99)00300-2.
- Hsu, H.-C., Sheu, Y.-W., Tu, C.-H., 2002. Viscosity estimation at low temperatures  $(T_r < 0.75)$  for organic liquids from group contributions. Chem. Eng. J. 88, 27–35. http://dx.doi.org/10.1016/S1385-8947(01)00249-2.
- Hukkerikar, A.S., Kalakul, S., Sarup, B., Young, D.M., Sin, G.A.r., Gani, R., 2012a. Estimation of environment-related properties of chemicals for design of sustainable processes: development of group-contribution+ (GC+) property models and uncertainty analysis. J. Chem. Inf. Model. 52 (11), 2823–2839. http://dx.doi.org/10.1021/ci300350r.

- Hukkerikar, A.S., Sarup, B., Ten Kate, A., Abildskov, J., Sin, G., Gani, R., 2012b. Group-contribution + (GC+) based estimation of properties of pure components: Improved property estimation and uncertainty analysis. Fluid Phase Equilib. 321, 25–43. http://dx.doi.org/10.1016/j.fluid.2012.02.010.
- Hutacharoen, P., Dufal, S., Papaioannou, V., Shanker, R.M., Adjiman, C.S., Jackson, G., Galindo, A., 2017. Predicting the solvation of organic compounds in aqueous environments: from alkanes and alcohols to pharmaceuticals. Ind. Eng. Chem. Res. 56 (38), 10856–10876.
- IEA, 2011. Climate Change 2021: The Physical Science Basis, Intergovernmental Panel on Climate Change. IEA Technical Report, OECD, URL https://www.ipcc.ch/report/ ar6/wg1/.
- IPCC, 2021. Climate Change 2021: The Physical Science Basis, Intergovernmental Panel on Climate Change. available at https://www.ipcc.ch/report/ar6/wg1/.
- Karunanithi, A.T., Achenie, L.E., Gani, R., 2006. A computer-aided molecular design framework for crystallization solvent design. Chem. Eng. Sci. 61 (4), 1247–1260. http://dx.doi.org/10.1016/j.ces.2005.08.031.
- Khalit, S.H., 2019. Development of SAFT-γ mie models for alkanolamines for carbon capture studies (Ph.D. thesis). Imperial College London.
- Klamt, A., Eckert, F., Arlt, W., 2010. COSMO-RS: An alternative to simulation for calculating thermodynamic properties of liquid mixtures. Annu. Rev. Chem. Biomol. Eng. 1 (1), 101–122. http://dx.doi.org/10.1146/annurev-chembioeng-073009-100903.
- Kocis, G.R., Grossmann, I.E., 1989. Computational experience with DICOPT solving MINLP problems in process systems engineering. Comput. Chem. Eng. 13 (3), 307–315. http://dx.doi.org/10.1016/0098-1354(89)85008-2.
- Kokossis, A.C., Yang, A., 2010. On the use of systems technologies and a systematic approach for the synthesis and the design of future biorefineries. Comput. Chem. Eng. 34 (9), 1397–1405. http://dx.doi.org/10.1016/j.compchemeng.2010.02.021.
- Lampe, M., Stavrou, M., Bucker, H., Gross, J., Bardow, A., 2014. Simultaneous optimization of working fluid and process for organic Rankine cycles using PC-SAFT. Ind. Eng. Chem. Res. 53 (21), 8821–8830. http://dx.doi.org/10.1021/ie5006542.
- Lampe, M., Stavrou, M., Schilling, J., Sauer, E., Gross, J., Bardow, A., 2015. Computer-aided molecular design in the continuous-molecular targeting framework using group-contribution PC-SAFT. Comput. Chem. Eng. 81, 278–287. http://dx.doi.org/10.1016/j.compchemeng.2015.04.008.
- Lee, Y.S., 2022. Multi-objective optimisation: algorithms and application to computer-aided molecular and process design (Ph.D. thesis). Imperial College London
- Lee, Y.S., Galindo, A., Jackson, G., Adjiman, C.S., 2021. An approach for simultaneous computer-aided solvent design and process design for CO<sub>2</sub> chemical absorption processes. In: Türkay, M., Gani, R. (Eds.), 31st European Symposium on Computer Aided Process Engineering. In: Computer Aided Chemical Engineering, Vol. 50, Elsevier, pp. 167–172. http://dx.doi.org/10.1016/B978-0-323-88506-5.50027-9.
- Lee, Y.S., Galindo, A., Jackson, G., Adjiman, C.S., 2023. A predictive modelling approach for CO<sub>2</sub> chemical absorption-desorption processes: linking solvent structure to techno-economic performance. Manuscript in Preparation.
- Lee, Y.S., Graham, E.J., Galindo, A., Jackson, G., Adjiman, C.S., 2020. A comparative study of multi-objective optimization methodologies for molecular and process design. Comput. Chem. Eng. 136, 106802. http://dx.doi.org/10.1016/j.compchemeng. 2020.106802.
- Mac Dowell, N., Galindo, A., Jackson, G., Adjiman, C., 2010. Integrated solvent and process design for the reactive separation of CO<sub>2</sub> from flue gas. In: Computer Aided Chemical Engineering. Vol. 28, Elsevier, pp. 1231–1236. http://dx.doi.org/ 10.1016/S1570-7946(10)28206-8.
- Maranas, C.D., 1997. Optimal molecular design under property prediction uncertainty. AIChE J. 43 (5), 1250–1264. http://dx.doi.org/10.1002/aic.690430514.
- Marrero, J., Gani, R., 2001. Group-contribution based estimation of pure component properties. Fluid Phase Equilib. 183, 183–208. http://dx.doi.org/10.1016/S0378-3812(01)00431-9.
- Mota-Martinez, M.T., Hallett, J.P., Mac Dowell, N., 2017. Solvent selection and design for CO<sub>2</sub> capture – how we might have been missing the point. Sustain. Energy Fuels 1, 2078–2090. http://dx.doi.org/10.1039/C7SE00404D.
- Muchan, P., Narku-Tetteh, J., Saiwan, C., Idem, R., Supap, T., Tontiwachwuthikul, P., 2017. Effect of number of hydroxyl group in sterically hindered alkanolamine on CO<sub>2</sub> capture activity. Energy Procedia 114, 1966–1972. http://dx.doi.org/10.1016/j.egypro.2017.03.1328.
- Ng, L.Y., Chong, F.K., Chemmangattuvalappil, N.G., 2015. Challenges and opportunities in computer-aided molecular design. Comput. Chem. Eng. 81, 115–129. http: //dx.doi.org/10.1016/j.compchemeng.2015.03.009.
- Odele, O., Macchietto, S., 1993. Computer aided molecular design: a novel method for optimal solvent selection. Fluid Phase Equilib. 82, 47–54. http://dx.doi.org/10. 1016/0378-3812(93)87127-M.
- Oyarzún, B., Bardow, A., Gross, J., 2011. Integration of process and solvent design towards a novel generation of CO<sub>2</sub> absorption capture systems. Energy Procedia 4, 282–290. http://dx.doi.org/10.1016/j.egypro.2011.01.053.
- Papadopoulos, A.I., Badr, S., Chremos, A., Forte, E., Zarogiannis, T., Seferlis, P., Papadokonstantakis, S., Galindo, A., Jackson, G., Adjiman, C.S., 2016. Computer-aided molecular design and selection of CO<sub>2</sub> capture solvents based on thermodynamics, reactivity and sustainability. Mol. Syst. Des. Eng. 1 (3), 313–334. http://dx.doi.org/10.1039/C6ME00049E.

- Papadopoulos, A.I., Linke, P., 2006a. Efficient integration of optimal solvent and process design using molecular clustering. Chem. Eng. Sci. 61 (19), 6316–6336. http://dx.doi.org/10.1016/j.ces.2006.06.006.
- Papadopoulos, A.I., Linke, P., 2006b. Multiobjective molecular design for integrated process-solvent systems synthesis. AIChE J. 52 (3), 1057–1070. http://dx.doi.org/ 10.1002/aic.10715.
- Papadopoulos, A.I., Perdomo, F.A., Tzirakis, F., Shavalieva, G., Tsivintzelis, I., Kazepidis, P., Nessi, E., Papadokonstantakis, S., Seferlis, P., Galindo, A., Jackson, G., Adjiman, C.S., 2021. Molecular engineering of sustainable phase-change solvents: from digital design to scaling-up for CO<sub>2</sub> capture. Chem. Eng. J. 420, 127624.
- Papadopoulos, A.I., Stijepovic, M., Linke, P., 2010. On the systematic design and selection of optimal working fluids for Organic Rankine Cycles. Appl. Therm. Eng. 30 (6–7), 760–769. http://dx.doi.org/10.1016/j.applthermaleng.2009.12.006.
- Papadopoulos, A.I., Stijepovic, M., Linke, P., Seferlis, P., Voutetakis, S., 2013. Toward optimum working fluid mixtures for organic rankine cycles using molecular design and sensitivity analysis. Ind. Eng. Chem. Res. 52 (34), 12116–12133. http://dx.doi.org/10.1021/je400968i.
- Papadopoulos, A.I., Tsivintzelis, I., Linke, P., Seferlis, P., 2018. Computer aided molecular design: Fundamentals, methods and applications. Chem. Mol. Sci. Chem. Eng. http://dx.doi.org/10.1016/B978-0-12-409547-2.14342-2.
- Papaioannou, V., Lafitte, T., Avendaño, C., Adjiman, C.S., Jackson, G., Müller, E.A., Galindo, A., 2014. Group contribution methodology based on the statistical associating fluid theory for heteronuclear molecules formed from Mie segments. J. Chem. Phys. 140 (5), http://dx.doi.org/10.1063/1.4851455.
- Perdomo, F.A., Khalit, S.H., Adjiman, C.S., Galindo, A., Jackson, G., 2021. Description of the thermodynamic properties and fluid-phase behavior of aqueous solutions of linear, branched, and cyclic amines. AIChE J. 67 (3), e17194. http://dx.doi.org/ 10.1002/aic.17194.
- Perdomo, F.A., Khalit, S.H., Graham, E.J., Tzirakis, F., Papadopoulos, A.I., Tsivintzelis, I., Seferlis, P., Adjiman, C.S., Jackson, G., Galindo, A., 2023. A predictive group-contribution framework for the thermodynamic modelling of CO<sub>2</sub> absorption in cyclic amines, alkyl polyamines, alkanolamines and phase-change amines: New data and SAFT-y mie parameters. Fluid Phase Equilib. 566, 113635. http://dx.doi.org/10.1016/j.fluid.2022.113635.
- Pereira, F.E., Jackson, G., Galindo, A., Adjiman, C.S., 2012. The HELD algorithm for multicomponent, multiphase equilibrium calculations with generic equations of state. Comput. Chem. Eng. 36, 99–118. http://dx.doi.org/10.1016/j.compchemeng. 2011.07.009.
- Pereira, F.E., Keskes, E., Galindo, A., Jackson, G., Adjiman, C.S., 2011. Integrated solvent and process design using a SAFT-VR thermodynamic description: High-pressure separation of carbon dioxide and methane. Comput. Chem. Eng. 35 (3), 474–491. http://dx.doi.org/10.1016/j.compchemeng.2010.06.016.
- Process Systems Engineering, 1997-2022. gPROMS ModelBuilder v 7.0.7. URL http://www.psenterprise.com/.
- Ramachandran, N., Aboudheir, A., Idem, R., Tontiwachwuthikul, P., 2006. Kinetics of the absorption of  $\rm CO_2$  into mixed aqueous loaded solutions of monoethanolamine and methyldiethanolamine. Ind. Eng. Chem. Res. 45 (8), 2608–2616. http://dx.doi.org/10.1021/ie0505716.
- Rennen, G., Van Dam, E.R., Den Hertog, D., 2011. Enhancement of sandwich algorithms for approximating higher-dimensional convex pareto sets. INFORMS J. Comput. 23 (4), 493–517. http://dx.doi.org/10.1287/ijoc.1100.0419.

- Rodriguez, J., Mac Dowell, N., Llovell, F., Adjiman, C., Jackson, G., Galindo, A., 2012. Modelling the fluid phase behaviour of aqueous mixtures of multifunctional alkanolamines and carbon dioxide using transferable parameters with the SAFT-VR approach. Mol. Phys. 110 (11–12), 1325–1348. http://dx.doi.org/10.1080/00268976.2012.665504.
- Roughton, B.C., Christian, B., White, J., Camarda, K.V., Gani, R., 2012. Simultaneous design of ionic liquid entrainers and energy efficient azeotropic separation processes. Comput. Chem. Eng. 42, 248–262. http://dx.doi.org/10.1016/j.compchemeng.2012.02.021.
- Russell, R., 1983. A flexible and reliable method solves single-tower and crude-distillation-column problems. Chem. Eng. (New York, NY) 90 (21), 52–59.
- Scheffczyk, J., Schäfer, P., Fleitmann, L., Thien, J., Redepenning, C., Leonhard, K., Marquardt, W., Bardow, A., 2018. COSMO-CAMPD: a framework for integrated design of molecules and processes based on COSMO-RS. Mol. Syst. Des. Eng. 3, 645–657. http://dx.doi.org/10.1039/C7ME00125H.
- Schilling, J., Horend, C., Bardow, A., 2020. Integrating superstructure-based design of molecules, processes, and flowsheets. AIChE J. 66 (5), e16903. http://dx.doi.org/ 10.1002/aic.16903.
- Schilling, J., Lampe, M., Gross, J., Bardow, A., 2017a. 1-stage CoMT-CAMD: An approach for integrated design of ORC process and working fluid using PC-SAFT. Chem. Eng. Sci. 159, 217–230. http://dx.doi.org/10.1016/j.ces.2016.04.048.
- Schilling, J., Tillmanns, D., Lampe, M., Hopp, M., Gross, J., Bardow, A., 2017b. From molecules to dollars: integrating molecular design into thermo-economic process design using consistent thermodynamic modeling. Mol. Syst. Des. Eng. 2, 301–320. http://dx.doi.org/10.1039/C7ME00026J.
- Silva-Beard, A., Flores-Tlacuahuac, A., Rivera-Toledo, M., 2022. Optimal computer-aided molecular design of ionic liquid mixtures for post-combustion carbon dioxide capture. Comput. Chem. Eng. 157, 107622. http://dx.doi.org/10.1016/j.compchemeng.2021.107622.
- Stavrou, M., Lampe, M., Bardow, A., Gross, J., 2014. Continuous molecular targeting-computer-aided molecular design (CoMT-CAMD) for simultaneous process and solvent design for CO<sub>2</sub> capture. Ind. Eng. Chem. Res. 53 (46), 18029–18041. http://dx.doi.org/10.1021/ie502924h.
- Stephenson, R.M., 1993. Mutual solubility of water and aliphatic amines. J. Chem. Eng. Data 38 (4), 625–629. http://dx.doi.org/10.1021/je00012a039.
- UNFCCC, 2015. Adoption of the Paris agreement. available at https://unfccc.int/resource/docs/2015/cop21/eng/109r01.pdf.
- Viswanathan, J., Grossmann, I.E., 1990. A combined penalty function and outer-approximation method for MINLP optimization. Comput. Chem. Eng. 14 (7), 769–782. http://dx.doi.org/10.1016/0098-1354(90)87085-4.
- Wang, X., Song, C., 2020. Carbon capture from flue gas and the atmosphere: A perspective. Front. Energy Res. 8, 560849.
- Zhang, S., Shen, Y., Wang, L., Chen, J., Lu, Y., 2019. Phase change solvents for post-combustion CO<sub>2</sub> capture: Principle, advances, and challenges. Appl. Energy 239, 876–897. http://dx.doi.org/10.1016/j.apenergy.2019.01.242.
- Zhou, T., Zhou, Y., Sundmacher, K., 2017. A hybrid stochastic-deterministic optimization approach for integrated solvent and process design. Chem. Eng. Sci. 159, 207–216. http://dx.doi.org/10.1016/j.ces.2016.03.011.